



Norwegian University of  
Science and Technology

# Direct Nonoxidative Conversion of Methane to C2 Hydrocarbons, Aromatics and Hydrogen

**Benedicte Hovd**

Chemical Engineering and Biotechnology

Submission date: June 2016

Supervisor: Hilde Johnsen Venvik, IKP

Co-supervisor: Anders Holmen, IKP

Bjørn Enger, SINTEF

Norwegian University of Science and Technology  
Department of Chemical Engineering



## PREFACE

---

The purpose of this work was to investigate the direct methane conversion based on results reported in Science 344 (6184), 616-619 by Guo et al. in the article "Direct, nonoxidative conversion of methane to C2 hydrocarbons, aromatics and hydrogen". An experimental setup was adapted to the direct methane conversion process, and the catalysts Fe@SiO<sub>2</sub> and Fe/HZSM-5 were prepared and their catalytic activity examined.

The project was conducted for the Master thesis in Catalysis at the Department of Chemical Engineering, NTNU.

Main supervisor at NTNU was Hilde Johnsen Venvik.

Assisting supervisor at NTNU was Anders Holmen.

I would like to express my gratitude towards Hilde Johnsen Venvik and Anders Holmen for their guidance throughout this master thesis. I would also like to thank Cristian Ledesma Rodriguez for his technical assistance.

## DECLARATION OF COMPLIANCE

I declare that this is an independent work according to the exam regulations of the Norwegian University of Science and Technology (NTNU).

Place and date:

Signature:

Trondheim, 09.06.2016

Benedicte Hovd

## ABSTRACT

---

Natural gas contains a large quantity of methane that is valuable as a fuel source. However, it can also be converted to light olefins, but the present synthesis route includes the conversion into synthesis gas. This is an extensive process that could benefit from being replaced by a more efficient direct conversion of methane. Several routes for direct conversion of methane has been developed, but none have proven to show the right degree of reactivity or selectivity that is required.

A new catalyst has been suggested in the article "Direct, nonoxidative conversion of methane to C<sub>2</sub> hydrocarbons, aromatics and hydrogen". The catalyst, which is claimed to have single iron sites, is reported to activate the C-H bond in methane, while at the same time preventing further dehydrogenation and C-C coupling. The selectivity to desired products was found to be over 99 %, and ethylene, benzene and naphthalene were the only products. Several other catalysts were also prepared, including the Fe/HZSM-5 catalyst. The product distribution obtained with this catalyst was promising, despite the formation of coke. The materials used to produce the Fe@SiO<sub>2</sub> catalyst were synthesized fayalite and silica. The fayalite and silica was ball milled, fused together and leached to create the catalyst. The Fe/HZSM-5 (1) catalyst was prepared by zeolite impregnation in an iron(III)nitrate solution, followed by calcination. Another catalyst, Fe/HZSM-5 (2), was prepared with the same materials, but with the more conventional incipient wetness impregnation method.

The activity of the catalysts was measured in a reactor using a total space velocity equal to that of Guo et al., and with nitrogen as an internal standard. The activity was measured at four temperatures, 1223, 1273, 1323 and 1373 K. Both Fe/HZSM-5 catalysts displayed activity at 1223 and 1273 K, obtaining significantly higher conversion than for the blank experiment (15-20 % opposed to 1 %). When the reactor temperature was increased to 1323 K the conversion for all four experiments was around 15 %. At 1373 K the conversion had a significant increase, ranging from 30-45 %. The highest conversion was obtained by a blank

experiment. The measurements at 1373 K were, however, unsure due to pressure buildup in the reactor, as a result of coke deposition on the catalysts.

As the reactor temperature increased, the selectivity towards acetylene increased as well. In fact, acetylene was observed for all measurements, which was a clear contradiction to the results from Guo et al. Higher hydrocarbons such as benzene and naphthalene could not be detected, and a more in depth analysis of the product stream should be conducted. The Fe@SiO<sub>2</sub> catalyst achieved the most desired product composition at 1323 K, having the highest selectivity towards ethylene and producing the least amount of coke. This proved that further examination of the Fe@SiO<sub>2</sub> catalyst should be pursued in order to reveal its true potential for methane conversion.

## SAMMENDRAG

---

Naturgass inneholder en store mengder metan. Metan er verdifull som en kilde til brensel, men kan også blir konvertert til basiskjemikalier. Dagens syntesemetode inkluderer konvertering av metan til syntesegass. Dette er en omfattende prosessrute som kan med fordel bli erstattet av en more effektiv direkte konvertering av metan. Flere prosesser har blitt utviklet, men ingen har vist den rette grad av reaktivitet eller selektivitet som er nødvendig.

En ny katalysator har blitt foreslått i artikkelen “Direct, nonoxidative conversion of methane to C2 hydrocarbons, aromatics and hydrogen”. Katalysatoren, som hevdes å ha enkle jern seter, er rapportert til å aktivere C-H bindingen i metan, mens den samtidig hindrer ytterligere dehydrogenering og C-C kobling. Selektiviteten til produkter som er ønsket i en slik prosess ble funnet til å være over 99 %. Etylen, benzen og naftalen var de eneste produktene. Det var rapportert at det ikke var noe koksdannelse på katalysatoren. Flere andre katalysatorer ble også laget, inklusiv Fe/HZSM-5 katalysatoren. Produktfordelingen som ble oppnådd med denne katalysatoren var lovende, selv om det var en god del koksdannelse. Materialene fayalitt og silika ble brukt til å produsere Fe@SiO<sub>2</sub> katalysatoren. Fayalitten var syntetisert og karakterisert ved XRD. Resultatene viste at prøven inneholdt fayalitt og FeO. Fayalitt og silika ble kulemøllt, smeltet sammen og utvasket for å lage katalysatoren. Fe/HZSM-5 (1) katalysatoren ble laget ved å impregnere zeolitt i en løsning av jern(III)nitrat, etterfulgt av kalsinering. Fe/HZSM-5 (2) katalysatoren ble laget ved den mer konvensjonelle «incipient wetness impregnation» metoden.

Aktiviteten til katalysatorene ble målt i en reaktor ved å bruke den samme volumhastigheten som Guo et al., og med nitrogen som intern standard. Aktiviteten ble målt ved 4 temperaturer, 1223, 1273, 1323 og 1373 K. Begge Fe/HZSM-5 katalysatorene viste aktivitet og selektivitet ved 1223 og 1273 K. Konverteringen var rundt 15-20 % som var betydelig høyere enn konverteringen som ble oppnådd i tom reaktor (1 %). Når reaktortemperaturen ble økt til 1323 K var konvertering av metan rundt 15 % for all eksperimentene. Ved 1373 K

økte konverteringen av metan betydelig, og varierte fra 30 til 45 %. Den høyeste konverteringen ble observert ved tom reaktor. Målingene ved 1373 K var imidlertid usikre på grunn av trykkoppbygning i reaktoren grunnet koksdannelse på katalysatoren.

Ved økt reaktortemperaturen, økte også selektiviteten mot acetylen. Det ble observert acetylen ved alle målingene som ble utført, som var en klar motsigelse til resultatene som ble rapportert av Guo et al. Høyere hydrokarboner kunne ikke bli detektert under analysen, og en mer grundig undersøkelse av produktstrømmen bør utføres. Men bortsett fra dette så ble den beste produktfordelingen oppnådd med Fe@SiO<sub>2</sub> katalysatoren. Selektiviteten mot etylene var høyest, og det ble produsert minst koks. Dette viser at videre undersøkelse av denne katalysatoren bør utføres for å oppdage dens reelle potensial for metan konvertering.

# TABLE OF CONTENT

---

Preface .....	i
Declaration of compliance .....	i
Abstract.....	ii
Sammendrag.....	iv
List of figures.....	1
List of tables .....	3
Abbreviations .....	4
1 Introduction.....	5
1.1 Scope of this work .....	5
2 Theory.....	6
2.1 Direct methane conversion.....	6
2.1.1 Oxidative coupling .....	6
2.1.2 Methane pyrolysis.....	7
2.1.3 Proposed Fe@SiO <sub>2</sub> catalyst.....	9
2.2 Reaction pathways.....	11
2.2.1 Ethylene reaction profile .....	11
2.2.2 Benzene reaction profile.....	12
2.2.3 Naphthalene reaction profile.....	14
2.3 catalyst preparation .....	15
2.3.1 Fe@SiO <sub>2</sub> .....	15
2.3.2 Fe/HZSM-5 .....	16
2.3.3 Zeolite structure and characteristics .....	18
2.4 Characterization techniques .....	21

2.4.1	X-ray diffraction .....	21
2.4.2	N <sub>2</sub> -adsorption.....	22
2.4.3	Other characterization methods.....	24
3	Experimental.....	26
3.1	Catalyst preparation.....	26
3.1.1	Fe@SiO <sub>2</sub> .....	26
3.1.2	Fe/HZSM-5 .....	27
3.2	Characterization .....	28
3.2.1	X-ray diffraction .....	28
3.2.2	N <sub>2</sub> -adsorption.....	29
3.3	Activity measurements .....	29
3.4	Activity analysis .....	32
4	Results and discussion .....	35
4.1	Catalyst synthesis .....	35
4.1.1	Fe@SiO <sub>2</sub> .....	37
4.1.2	Fe/HZSM-5 .....	39
4.2	Catalyst characterization.....	40
4.3	Reaction set-up .....	42
4.4	Catalyst activity .....	43
5	Future work .....	60
6	Conclusion .....	61
	References .....	63
	Appendix A - Flow controller calibration .....	I
	Appendix B – μGC Calibration.....	II

Appendix C - Separation of acetylene and ethylene .....	III
Appendix D – Risk evaluation .....	VI

## LIST OF FIGURES

---

Figure 1: The equilibrium composition of the C-H system as a function of temperature. Coke and polycyclic aromatic products (except naphthalene) are excluded. [9] .....	8
Figure 2: The nonoxidative direct conversion catalyst, Fe@SiO <sub>2</sub> , developed by Guo et al. [5]	9
Figure 3: The conversion and selectivity obtained at different reaction temperatures and space velocities. The conversion is marked in blue, while the bars represent product selectivity. [4].....	10
Figure 4: Reaction mechanism for the direct conversion of methane using the Fe@SiO <sub>2</sub> catalyst.[5].....	11
Figure 5: The radical transformation that occurs in the reaction profile. [4].....	13
Figure 6: Termination of the radical reaction during benzene formation. [4] .....	14
Figure 7: The radical transformation phase in the reaction of benzene to naphthalene.[4].	15
Figure 8: Termination of the radical reaction during naphthalene formation. [4] .....	15
Figure 9: Product distribution obtained by different iron based catalysts at 1223 K.[4] .....	17
Figure 10: The tetrahedra geometry of AlO <sub>4</sub> and SiO <sub>4</sub> that make up the basic building blocks of zeolites. [16] .....	19
Figure 11: Example of a zeolite structure. The edges are made up of Si or Al ions, which are connected by oxygen ions in-between the corners. [17] .....	20
Figure 12: Examples of how zeolites can alter selectivity based on reactant/product/intermediate shape. [15].....	21
Figure 13: An illustration of the scattered X-ray photons that determine the crystallinity of a sample. [19] .....	22
Figure 14: BET isotherms. [22].....	24
Figure 15: Setup in the high temperature furnace. ....	27
Figure 16: Catalyst preparation setup. ....	28
Figure 17: Schematic of the experimental setup involving the reactor used for the activity measurements. ....	30
Figure 18: Schematic of the reactor used for the activity measurements. ....	31
Figure 19: XRD plot for the synthesized fayalite with an overlay of pure fayalite. ....	36

Figure 20: XRD plot of the synthesized fayalite with an overlay of FeO. ....	36
Figure 21: The result from fusing together the powders in the high temperature furnace. .	38
Figure 22: Fe/HZSM-5 catalyst mixture” .....	39
Figure 23: Catalyst before crushing with mortar.....	40
Figure 24: The methane conversion obtained with the prepared catalysts and empty reactor experiments. ....	45
Figure 25: Hydrogen flow in product stream.....	46
Figure 26: Fe@SiO <sub>2</sub> catalyst and monolith after the experiments.....	48
Figure 27: product distribution at 1223 K. The associated methane conversion level is displayed linearly in the diagram.....	50
Figure 28: Product distribution at 1323 K for the 3 different catalysts. The associated methane conversion level is displayed linearly in the diagram. ....	51
Figure 29: Reactor before and after. ....	53
Figure 30: The estimated hydrogen loss for the four experiments.....	54
Figure 31: Ethylene selectivity obtained for the four experiments.....	55
Figure 32: Acetylene selectivity obtained for the four experiments.....	55
Figure 33: Selectivity vs conversion .....	56
Figure 34: The response area for ethylene and acetylene is compared in the figure.....	57
Figure 35: The Fe/HZSM-5 catalyst methane conversion analyzed from low temperature to high, and opposite. ....	59

## LIST OF TABLES

---

Table 1: The catalysts used for the five activity measurements .....	29
Table 2: An overview of the total space velocity used for each reactor temperature.....	30
Table 3: Column types in the Agilent 3000a $\mu$ GC. ....	32
Table 4: N <sub>2</sub> -adsorption results .....	41

## ABBREVIATIONS

---

<b>BET</b>	Brunauer Emmet and Teller
<b>DFT</b>	Density functional theory
<b>EXAFS</b>	X-ray absorption fine structure
<b>HAADF</b>	High-angle annular dark field
<b>MDA</b>	Methane dehydroaromatization
<b>MTH</b>	Methanol-to-hydrocarbon
<b>OCM</b>	Oxidative coupling of methane
<b>STEM</b>	Scanning transmission electron microscopy
<b>TPD-NH<sub>3</sub></b>	Temperature programmed desorption
<b>VUV-SPI-MBMS</b>	Vacuum ultraviolet soft photoionization molecular-beam mass spectrometry
<b>XRD</b>	X-ray diffraction
<b>XPS</b>	X-ray photoelectron spectroscopy

# 1 INTRODUCTION

---

The increased demand for efficient use of the worlds energy resources has motivated the search for a less complicated route for converting natural gas to valuable products, such as base chemicals. Methane has a high H/C ratio, which is underutilized in the industry today. The increased production of shale gas in the United States is of one the contributing factors for the increased interest in methane conversion. [1]

Natural gas mainly consists of methane, usually between 70-90 volume %. The main use of methane is for fuel, but a great deal of natural gas resources is found in places where gas transportation is not a valid alternative. The conversion of methane to other products is therefore a valuable route for the exploitation of natural gas. [2, 3]

Light olefins from methane are currently obtained by converting methane into synthesis gas, which is subsequently converted into methanol, which through the methanol-to-hydrocarbon (MTH) process can form light olefins. This process requires several steps, and is both energy intensive and expensive. It is however a viable route for converting methane and is industrially utilized today. An alternative to the synthesis gas route is direct conversion of methane. This route is however not commercially sustainable at the current time. [3-6]

## 1.1 SCOPE OF THIS WORK

The work in this project was mainly focused on investigating the findings into direct methane conversion obtained by Guo et al. in the research paper "*Direct conversion of methane to C<sub>2</sub> hydrocarbons, aromatics and hydrogen*". The catalysts Fe@SiO<sub>2</sub> and Fe/HZSM-5 are to be synthesized as well as measured for activity. To accomplish this an experimental set-up has to be established to fit the needs of the high temperature methane conversion reaction.

## 2 THEORY

---

### 2.1 DIRECT METHANE CONVERSION

The research into direct methane conversion has been extensive. However, no ideal process has been developed. Due to the strong C-H bonds in methane ( $439 \text{ kJ mol}^{-1}$ ), splitting the bonds will require a very high temperature. In fact, the C-H bonds in methane are stronger than those in the resulting products. Achieving an adequate selectivity is therefore a challenge. Catalysts can lower the required temperature down to around 1073 K, but this is still viewed as a high-temperature process. For the last three decades the research into direct methane conversion has been centered around solving the obstacles of thermodynamically limited conversion and difficulty with product selectivity. Another prominent problem with catalytic methane conversion is the deactivation of the catalyst due to coke deposition. [7]

#### 2.1.1 Oxidative coupling

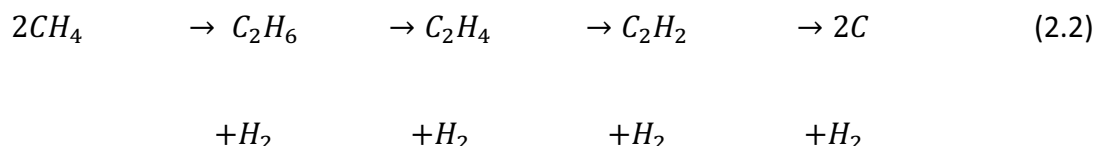
Methane can react with oxygen over a catalyst in a process called oxidative coupling of methane (OCM). The reaction consists of methyl radicals forming on the catalyst surface, which will enter the gas phase and combine together to ethane. Dehydrogenation of ethane leads to the formation of ethylene. However, the products can also be activated by the catalysts, which leads to the formation of  $\text{CO}_2$ .  $\text{C}_2$  yields of about 25 % has been obtained, and it is suggested that the maximum theoretical yield is 30 %. The oxidative coupling process does not achieve a satisfying selectivity for commercial use. [3, 5, 6] The global reaction that occur during OCM is shown below (equation 2.1). The reaction is exothermic as displayed by the heat of formation, and as a result the oxidative conversion is more thermodynamically favorable than nonoxidative conversion. [7, 8]



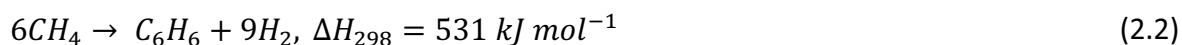
The side reactions that can occur produces CO and  $\text{CO}_2$  in exothermic reactions. This requires removal of heat from the reactor, which adds to the disadvantages of the OMC process. [3]

### 2.1.2 Methane pyrolysis

Another direct conversion route is the pyrolysis of methane. Performed at high temperature this process will give products such as acetylene. The reaction time is kept short, and the temperature very high (> 2000 K). The reaction consists of radical reactions in the gas phase, that can be summed up as stepwise dehydrogenation: [3]



Catalytic pyrolysis of methane is also developed for lower temperatures. This process is referred to as methane dehydroaromatization (MDA). The process is endothermic and requires a high amount of heat. A global representation of the process is shown in equation 2.2. At 973 K an equilibrium conversion of 12 % is attainable, while an equilibrium conversion of 24 % can be obtained at 1073 K. The catalysts are bifunctional and usually zeolite based. Mo/HZSM-5 is a catalyst that has received a lot of attention, though other transition metal ions have also shown activity towards MDA. It is suggested that methane will be converted into ethylene on molybdenum carbide or oxycarbide, which will be subsequently converted to aromatic products on the acidic sites inside the zeolite. Benzene is a desired product which is important as a feedstock for phenol and *p*-xylene. Brønsted acidic sites are important for the catalytic activity of MDA catalysts, and the Si/Al ratio of the zeolite can be varied to obtain a more optimal amount of Brønsted acidic sites. [3, 6]



The main products reported at a reactor temperature of 973 K are benzene and naphthalene. Figure 1 shows the effect of the temperature on the equilibrium composition on the C-H system. [6] A great benefit of nonoxidative conversion is the production of clean hydrogen. The hydrogen from this reaction is of high value, and due to the nonoxidative conditions there is no formation of carbon oxides. However, due to the low conversion the product stream

will also contain methane which must be separated before the hydrogen can be readily used in fuel cells. All though the cleanest way to produce hydrogen is from water electrolysis, a process utilizing this concept has not been developed to an industry standard yet. The high atomic H/C ratio in methane makes it an excellent source for hydrogen. The further development of the MDA process could therefore give rise to an important hydrogen source. [8]

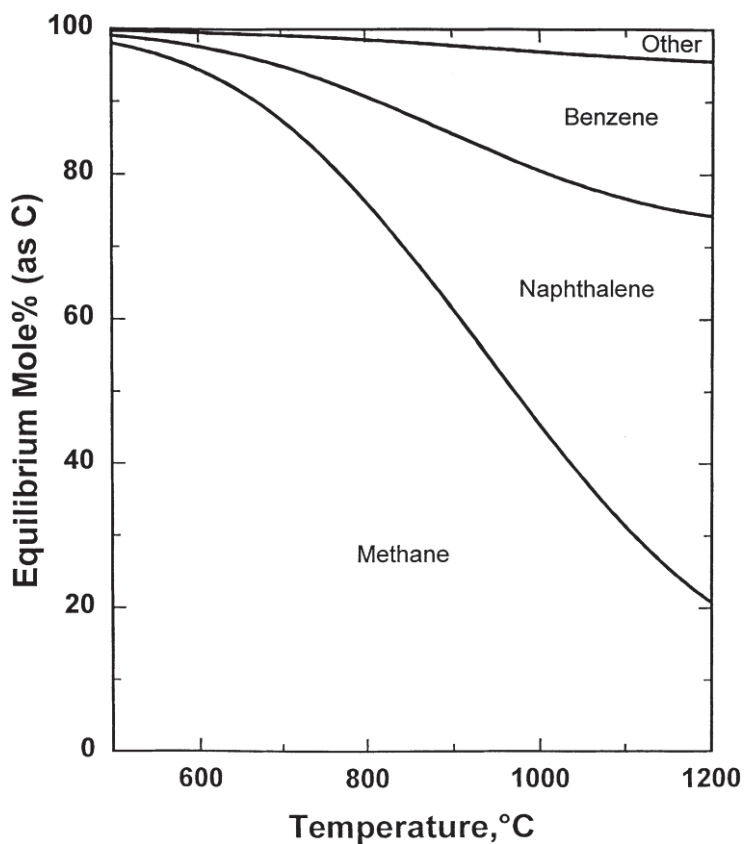


Figure 1: The equilibrium composition of the C-H system as a function of temperature. Coke and polycyclic aromatic products (except naphthalene) are excluded. [9]

Coupling methane with membrane technology has also proved successful in enhancing the methane conversion. By using hydrogen selective membranes together with a Mo/HZSM-5 catalyst, the formation of benzene, toluene, naphthalene and hydrogen was increased. [3]

The main deactivation source for the MDA catalysts is the deposition of coke on the surface, and several recent studies have been focused on increasing the stability. Coking will inhibit formation of complexes inside the zeolite pores, effectively decreasing the catalyst stability over time. The research into avoiding this deactivation include the addition of CO/CO<sub>2</sub> to the feed stream and treating the catalyst with steam. [3, 8]

### 2.1.3 Proposed Fe@SiO<sub>2</sub> catalyst

A study performed by Guo et al. [4] in 2013 has provided a new insight into the non-oxidative conversion of methane. By using a catalyst with single iron sites that is embedded into a silica matrix, it is suggested that coke deposition can be avoided completely, and the resulting products were exclusively ethylene and aromatics. An illustration of the catalyst is shown in Figure 2. The authors of the article have emphasized the catalysts ability to prevent C-C coupling, attributed to the single iron sites, which explains the absence of coke formation on the catalyst. The single iron sites were characterized by X-ray absorption fine structure (EXAFS) and high-angle annular dark field (HAADF) scanning transmission electron microscopy (STEM) measurements. [4, 5]

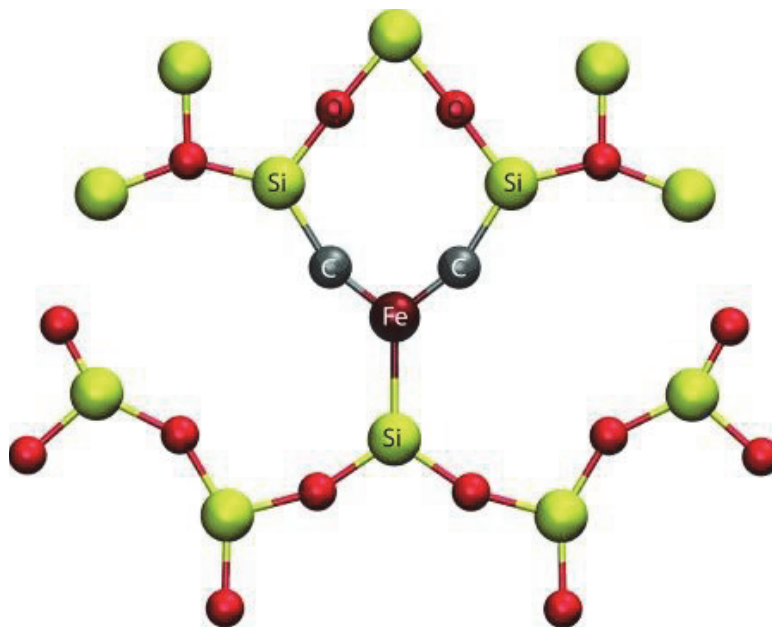


Figure 2: The nonoxidative direct conversion catalyst, Fe@SiO<sub>2</sub>, developed by Guo et al. [5]

The catalyst works by activating the first C-H bond in methane, and at the same time inhibiting even further dehydrogenation. At the reaction temperature of 1363 K a conversion of 48 % was reported. A long term test was also initiated, which showed that during the 60 hours testing period at 1293 K no deactivation of the catalyst occurred. This process might also have a significant value to the production of H<sub>2</sub>, seeing as no CO or CO<sub>2</sub> was formed. The article also puts emphasis on the lack of acetylene obtained from this process. Compared to products obtained from previous direct methane conversion techniques this is a favorable result. [4]

The product distribution obtained as a function of reactor temperature is shown in Figure 3. As expected, the methane conversion increased with increasing reactor temperature. The methane conversion obtained in the article reached 48 % at the temperature 1363 K. The product selectivity towards ethylene, naphthalene and benzene was constantly over 99 % for all reactor temperatures. The conversion and selectivity were calculated from the carbon balance. [4]

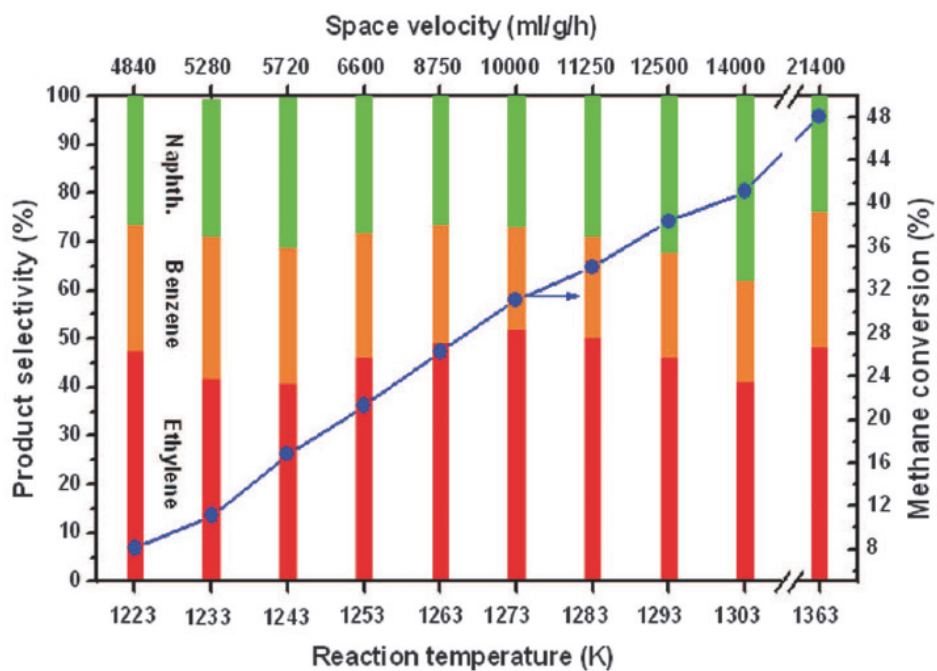


Figure 3: The conversion and selectivity obtained at different reaction temperatures and space velocities. The conversion is marked in blue, while the bars represent product selectivity. [4]

The catalyst was prepared by ball-milling fayalite ( $\text{Fe}_2\text{SiO}_4$ ) and silica together, fusing the mixture together at 1973 K in air, and lastly leaching the catalyst with nitric acid. [4]

## 2.2 REACTION PATHWAYS

The reaction pathway for the direct conversion of methane using the  $\text{Fe@SiO}_2$  catalyst is proposed to start with the generation of methyl radicals. Guo et al. [4] used density functional theory (DFT) calculations to calculate the bond dissociation energies. The DFT calculations were based on the results from vacuum ultraviolet soft photoionization molecular-beam mass spectrometry (VUV-SPI-MBMS), which was used to identify the methyl radicals in the gas phase. Figure 4 shows the proposed overall reaction mechanism. [4, 5]

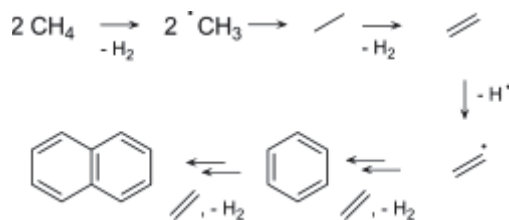


Figure 4: Reaction mechanism for the direct conversion of methane using the  $\text{Fe@SiO}_2$  catalyst. [5]

Three reaction profiles were suggested to show the formation of ethylene, benzene and naphthalene. [4]

### 2.2.1 Ethylene reaction profile

The overall reaction for the formation of ethylene can be written as:



The methyl radicals will enter the gas phase and recombine to ethane:



Ethane will dehydrogenate to ethylene, which can occur through three different pathways.

Pathway A consists of two bond dissociations:



Pathway B uses a  $CH_3^\bullet$  radical to form  $C_2H_5$ :



Pathway C occurs by dehydrogenation of ethane that is catalyzed by a H radical.



Guo et al. [4] proposes that these reactions are the reason why no ethane is observed in their experiments. The ethylene can undergo hydrogen abstraction to form  $^*C_2H_3$  radicals, that can react with ethane and eventually form benzene. Benzene can after several reaction steps form naphthalene. [4]

### 2.2.2 Benzene reaction profile

The overall reaction profile for the formation of benzene is shown in equation 2.11. The reaction is based on radicals, and is proposed to consist of radical generation, transformation and termination.



The radical  $C_2H_3$  has two suggested generation paths, as shown in equation 2.12 and 2.13.



During the radical transformation the generated radical  $C_2H_3$  will react together with two ethylene molecules, that after dehydrogenation and cyclization will yield  $C_6H_7$ . The reaction mechanisms are shown in Figure 5.

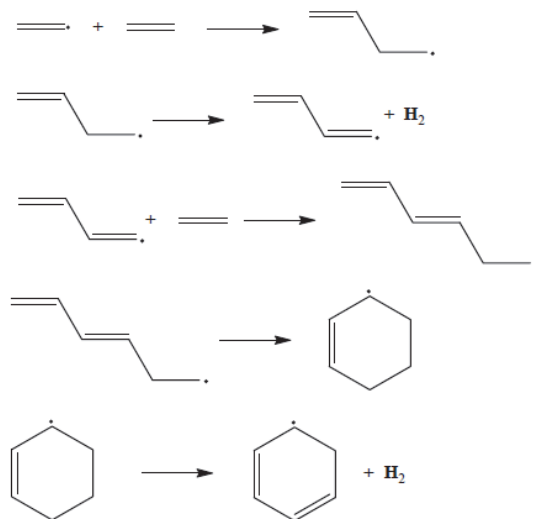


Figure 5: The radical transformation that occurs in the reaction profile. [4]

The reaction is terminated by the dissociation of a C-H bond from the  $C_6H_7$  molecule which results in the formation of benzene, as demonstrated in Figure 6.

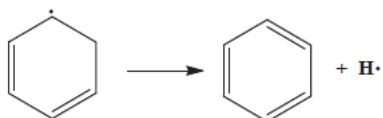
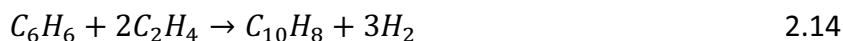


Figure 6: Termination of the radical reaction during benzene formation. [4]

Guo et al. [4] reports that the formation of ethylene occurs more easily than the transformation, which explains the accumulation of ethylene during the reaction. [4]

### 2.2.3 Naphthalene reaction profile

The naphthalene reaction profile is similar to the formation of benzene; it also consists of a radical generation, transformation and termination. The overall reaction is shown in equation 2.14.



There are two possibilities for the formation of radicals from benzene.



The radical formed from benzene can then react with ethylene, before going through dehydrogenation and cyclization to form  $C_{10}H_9$ , as shown in Figure 7.

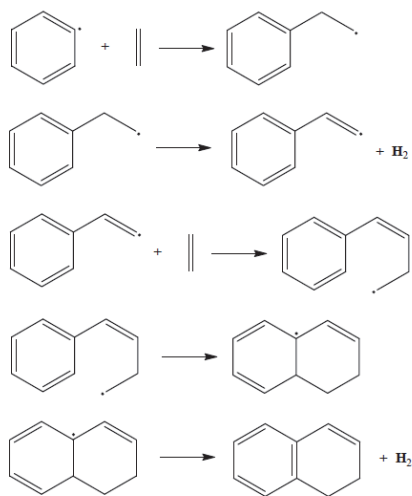


Figure 7: The radical transformation phase in the reaction of benzene to naphthalene. [4]

The radical termination consists of the dissociation of a C-H bond from the  $C_{10}H_9$  molecule as demonstrated in Figure 8.

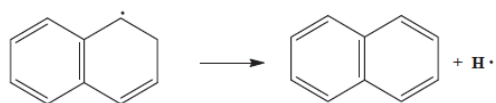


Figure 8: Termination of the radical reaction during naphthalene formation. [4]

The formation of benzene occurs more easily than its abstraction into naphthalene, which allows the buildup of benzene during the reaction. [4]

## 2.3 CATALYST PREPARATION

### 2.3.1 Fe@SiO<sub>2</sub>

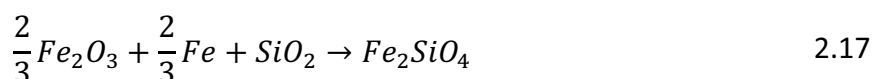
The unusual catalyst synthesis method employed by Guo et al. [4] can be summarized into 4 steps:

1. Mix 6 g SiO<sub>2</sub> with 112 mg Fe<sub>2</sub>SiO<sub>4</sub> and subject to ball milling (450 rev/min) for 15 h under high purity argon.
2. Fuse the mixture together at 1973 K for 6 h in air.

3. Leach using aqueous HNO<sub>3</sub> (0.5 M)
4. Dry at 353 K for 12 h.

The iron loading of the catalyst was 0.5 %. [4]

Fayalite, Fe<sub>2</sub>SiO<sub>4</sub>, is a naturally occurring mineral that also can be synthesised. Research into fayalite studies showed that there was a wide spread in the synthesis method employed by each study. [10-12] Akimoto and Fujisawa made pure fayalite with an olivine structure. [12] Solid-state reaction techniques were employed under a controlled atmosphere. Carefully synthesised FeO and SiO<sub>2</sub> were ground together, and heated at 1523 K at an oxygen partial pressure of 10<sup>-9.01</sup> atm. The mixture was grounded and heated again, and was determined to be a single phase material. Chen et al. [10] synthesised fayalite by mixing oxides at atmospheric pressure. Fe<sub>2</sub>O<sub>3</sub> and silica were baked to drive off moisture, before they were weighed out in stoichiometric amounts to form fayalite. The powders were ground in ethanol, pressed into pellets, and sintered at 1273 K for 1 day. This process was completed 3 times, before the fayalite was hot-pressed into disks. [10] D. Daval et al. [11] provided a third option for the synthesis of fayalite. Fe, Fe<sub>2</sub>O<sub>3</sub> and SiO<sub>2</sub> powders were ball milled thoroughly for 30 minutes under argon atmosphere, and then heated to 1023 K for 24 hours to form fayalite. The powders reacted together according to the following equation: [11]



X-ray diffraction (XRD) was used to investigate if the produced product was likely to consist of fayalite. [13]

### 2.3.2 Fe/HZSM-5

In addition to the Fe@SiO<sub>2</sub> catalyst, a range of other Fe catalysts were also synthesized and measured for activity towards methane conversion by Guo et al. [4] As illustrated in Figure 9, the product distribution obtained differed greatly between the catalysts used. However, they

all had coke formation on the catalyst as a common denominator. This is believed to be due to the difference in structure of the catalysts. Whereas the Fe@SiO<sub>2</sub> consisted of an isolated iron atom, the other catalysts could not achieve this structure to the same extent. Despite producing a fair amount of coke, the Fe/HZSM-5 catalyst showed promising selectivity towards ethylene and aromatics with a reactor temperature of 1223 K. Similar to the results obtained with the Fe@SiO<sub>2</sub> catalyst, no acetylene was produced for any of the catalysts used at this reactor temperature. [4]

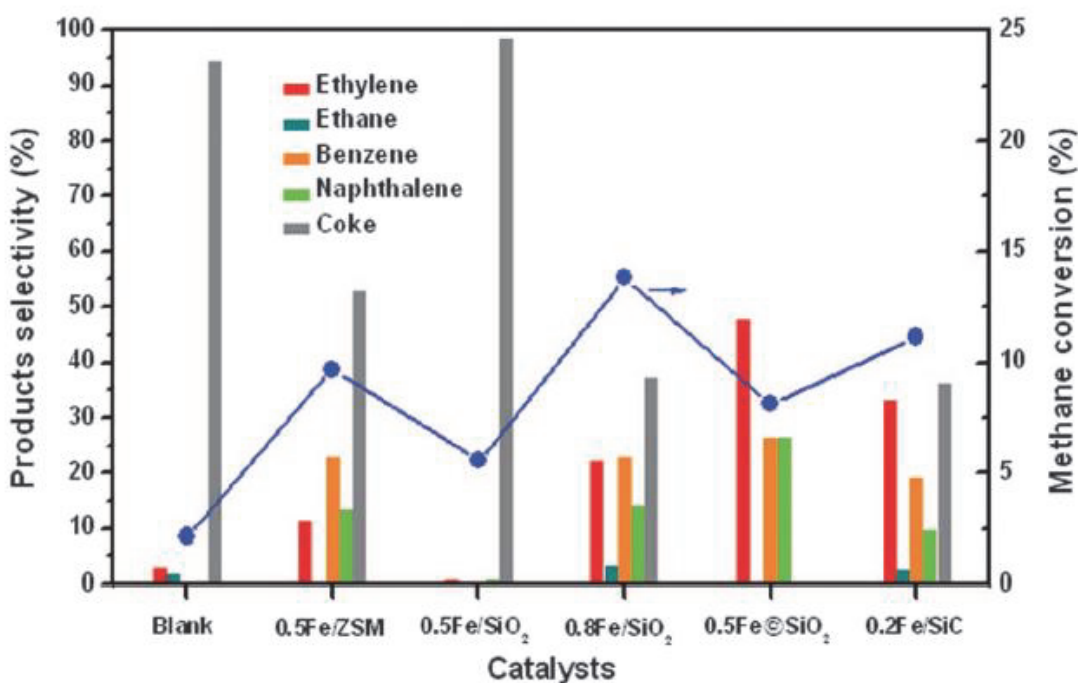


Figure 9: Product distribution obtained by different iron based catalysts at 1223 K.[4]

The preparation of the Fe/HZSM-5 catalyst included an impregnation method. The Fe loading of the catalyst was 0.5 wt. %. The preparation procedure was as following: [4]

1. Add 5.2 mL aqueous nitric acid (0.11 M) to 6 g of HZSM-5 zeolite.
2. Stir for 12 hours at ambient temperature.
3. Stir for 24 hours at 333 K.
4. Calcine the solid at 823 K for 6 hours.

A comparable catalyst was prepared by Tan [14]. Even though the catalyst was used for a lower temperature aromatization of methane, the preparation method shared many similarities. The zeolite was impregnated with Fe from an iron(III)nitrate solution, followed by drying at 393 K and calcination at 723 K. The zeolite used had a different Si/Al ratio (25 opposed to 15) and the temperatures varied slightly. Nonetheless, the preparation method was deemed to be within a suitable range for comparison with the catalyst in this project. The catalyst prepared by Tan [14] was subjected to several characterization methods to investigate the effect of the Fe loading on the zeolite. Among these characterization methods were N<sub>2</sub>-adsorption measurements to evaluate the effect of the Fe loading on the surface area. The pore volume was also compared based on these measurements. Tan [14] found that as the Fe loading on the zeolite increased, the BET surface area decreased while the average pore size increased. It was also reported that the microporous surface and volume decreased while the external surface area increased. From these results it was hypothesized that the Fe loading on the catalyst did not block the zeolite channels, and that the Fe instead migrated into the pores of the zeolite, which would result in a lower microporous surface area and volume. [14]

### 2.3.3 Zeolite structure and characteristics

The term zeolite was originally coined in 1756 by a Swedish mineralogist when he discovered “an unknown species of rock”. Zeolites are characterized by their microporous structure, and occur naturally, but they can also be synthesized. The tetrahedral SiO<sub>4</sub> and AlO<sub>4</sub> (Figure 10) make up the structure of zeolites. The corner oxygen atoms are shared between the two oxides, which forms the unique crystalline structure of the zeolite. Zeolites have a wide range of applications, the most commonly known use is in detergents. But their acidic properties also make them excellent as catalysts. In the 1960s it was discovered that faujistic zeolites showed promise as solid acid catalysts, and since then the catalytic properties of zeolites have been extensively researched and documented. A clear benefit when using zeolites is that the catalytic sites are well defined, due to the well-known crystallite structure of zeolites. Zeolites that occur naturally are usually named after the geographical location of where they were

found or by who discovered it, while synthetic zeolites are given their name by the industry or university where they were developed. An example of this is Bikitaite that was found in Bikita, Zimbabwe, and VPI that was developed at Virginia Polytechnic Institute. [15]

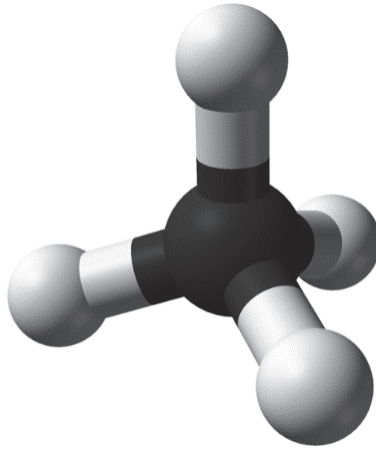


*Figure 10: The tetrahedra geometry of  $AlO_4$  and  $SiO_4$  that make up the basic building blocks of zeolites. [16]*

Over 600 zeolites structures have been documented, and new ones are continuously being discovered. As mentioned,  $SiO_4$  and  $AlO_4$  bound together by sharing oxygen atoms form the zeolite structure. The oxides can bond together in several different ways, resulting in a wide range of different zeolite structures. By forming squares or six and eight membered rings the tetrahedra can form together and create building blocks. These building blocks can then be arranged into periodic structures that make up the structure of the zeolite, as shown in Figure 11. [15]

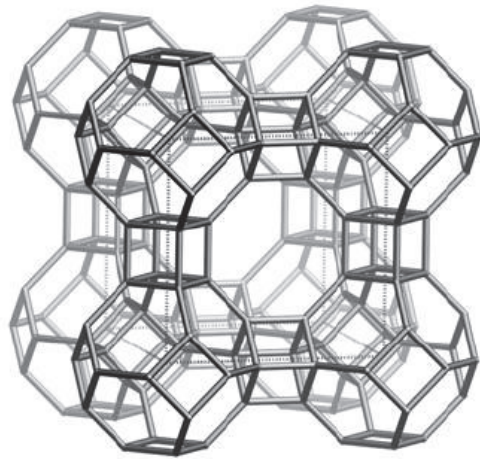


*Figure 11: Example of a zeolite structure. The edges are made up of Si or Al ions, which are connected by oxygen ions in-between the corners. [17]*

The hydrothermal synthesis of zeolites occurs in pressurized autoclaves. Template molecules are added to the mixture as structure directing agents. By replacing a  $\text{Si}^{4+}$  ion with an  $\text{Al}^{3+}$  ion the tetrahedra obtains a negative charge of -1. This charge can be neutralized by adding cations, which also can be replaced by protons, resulting in a polyacid. The zeolite will then be given the name H-X or H-ZSM-5, etc. (the H denotes the proton). By protonating the oxygen in the Si-O-Al bridge the zeolite obtains a strong Brønsted acidity. The surrounding ions, especially other aluminum ions, affect the strength of the Brønsted acid site. [15, 18]

Zeolites also have ion exchange capabilities, which is the reason the largest application for zeolites is as builders in detergent. Zeolite in sodium form will interchange its sodium ion with calcium and magnesium. [15]

The structure of the zeolite, as well as its acidic sites makes it ideal for catalysis. The uniform pore systems and pore channels contributes to the activity of zeolites by acting as molecular sieves. The intricate pore system can achieve better selectivity for a desired product by for example inhibiting the entrance of a reactant into the zeolite. Figure 12 shows how the zeolite can impact the selectivity of a reaction. In the first case only reactant A can enter the zeolite. For the second case two products are formed in the reaction, but only product B possesses

the right shape to leave the zeolite, effectively increasing its selectivity. In the last case A reacts to B, which also can react further to C. As for the second case, C is too large to leave the zeolite pores and its production will therefore be inhibited. [15, 18]

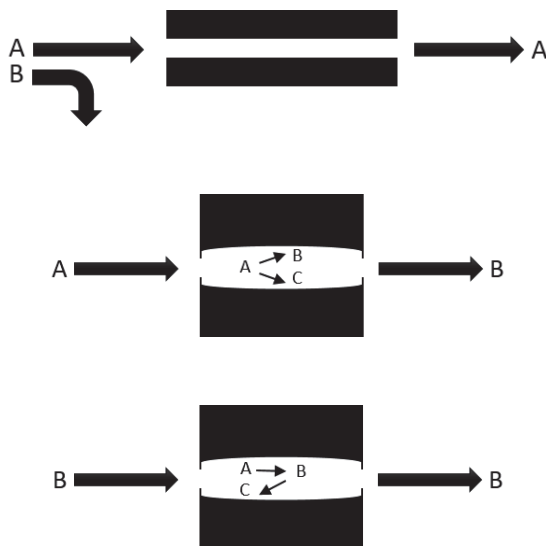


Figure 12: Examples of how zeolites can alter selectivity based on reactant/product/intermediate shape. [15]

The HZSM-5 catalyst has been documented to produce aromatics as one of its main products from olefins. This zeolite is often applied in aromatic chemistry, such as in the Selective Toluene Disproportionation process, increasing the selectivity towards benzene and paraxylene from toluene. HZSM-5 is often also used for aromatization of paraffins due to the product selectivity it can obtain. In this kind of reaction is accompanied by a dehydrogenation component, such as Pt or Zn. Other uses for HZSM-5 based catalysts are for the MTH process, the Lurgi Methanol to Propylene process. HZSM-5 has also recently been used as a component in fluid catalytic cracking catalysts. [18]

## 2.4 CHARACTERIZATION TECHNIQUES

### 2.4.1 X-ray diffraction

XRD is a well-known and often used technique for characterizing materials. By bombarding a sample with electrons, the scattering of the X-ray photons can be used to determine the

crystallinity of the sample. Figure 13 shows how the angles of the diffracted beams are defined. By measuring the angle  $2\theta$ , the Bragg's relation (equation 2.18) can be used to find the distance between the lattice planes. The spacing between the lattice planes is unique for a particular compound, and can therefore be used to distinguish which crystalline compounds are in the sample. [15]

$$n\lambda = 2d\sin\theta, n = 1, 2, \dots \quad 2.18$$

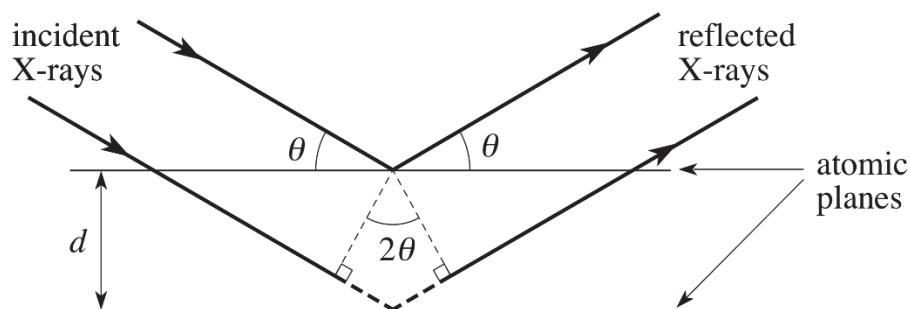


Figure 13: An illustration of the scattered X-ray photons that determine the crystallinity of a sample. [19]

The XRD characterization method does have its limits. The sample needs to be crystalline enough to diffract the X-rays, and must be present in a large enough quantity. It cannot detect amorphous or very small ( $< 2 \text{ nm}$ ) particles. [15]

#### 2.4.2 $\text{N}_2$ -adsorption

The surface area of a solid catalyst can be measured by  $\text{N}_2$ -adsorption. At 77 K the area of a  $\text{N}_2$  molecule occupies on the surface is known to be  $0.162 \text{ nm}^2$ . When the total surface is covered by  $\text{N}_2$  molecules the surface area can be derived. However, the  $\text{N}_2$  molecules has the possibility to adsorb in multilayers which complicates the calculations. The  $\text{N}_2$  molecules may also condense in small pores. The Kelvin equation is often applied to calculate the pore size and distribution of the solid material. The Brunauer Emmet and Teller (BET) isotherm

describes the physical adsorption of gas molecules onto the surface, and is used to calculate the surface area. The BET equation is shown below (equation 2.19).

$$\frac{1}{\left[V_a \left(\frac{P_0}{P} - 1\right)\right]} = \frac{C - 1}{V_m C} \frac{P}{P_0} + \frac{1}{V_m C} \quad 2.19$$

Where,

P = partial vapour pressure of adsorbate gas in equilibrium [Pa]

P<sub>0</sub> = equilibrium pressure [Pa]

V<sub>a</sub> = Volume of adsorbed gas at STP [mL]

V<sub>m</sub> = Volume of adsorbed gas at STP to produce an apparent monolayer on the sample surface [mL]

C = Dimensionless constant

The customary preparation of a sample for N<sub>2</sub>-adsorption includes heating to evaporate water while concurrently evacuating the sample. The sample is then placed in a chamber where it is cooled by liquid nitrogen at 77 K. An adsorptive, usually nitrogen is added to the solid in controlled doses. After the addition of the adsorptive, and the pressure has equilibrated, the amount that has adsorbed on the surface is calculated. The adsorption isotherm can vary depending on the category of material that is measured, as shown in Figure 14. [15, 20, 21]

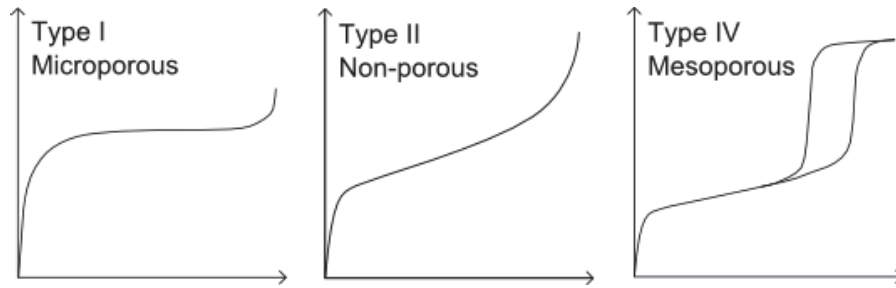


Figure 14: BET isotherms. [22]

However, there are a few assumptions that must be taken into account for the BET theory to be valid: [15]

- There is a dynamic equilibrium between adsorbate and adsorptive, resulting in an equal rate of adsorption and desorption.
- For the first layer of adsorption, the molecules will adsorb on comparable adsorption sites.
- The molecules in a consecutive layer will adsorb onto the molecules from the previous layer.
- Interaction between adsorbates is discounted.
- The conditions for adsorption-desorption are the same for all layers except the first.
- After the first layer the adsorption energy for molecules is equal to the condensation energy.
- When  $P = P_0$  the multilayer will grow to an infinite thickness.

#### 2.4.3 Other characterization methods

Guo et al. [4] employed a range of different characterization methods to examine the Fe@SiO<sub>2</sub> catalyst. EXAFS was employed to estimate the bond length between Si-C and Si-Fe. When the adsorbing atom is exposed to X-rays, the resulting scattering of photoelectrons by neighboring atoms creates interference in the X-ray absorption spectrum. By using this technique, information such as distance, number and type regarding the neighboring atoms

of the absorbing atom can be found. STEM-HAADF was used by Guo et al. [4] to characterize the isolated iron sites on the Fe@SiO<sub>2</sub> catalyst. [4, 15]

These characterization methods were not available for use in this project.

## 3 EXPERIMENTAL

---

### 3.1 CATALYST PREPARATION

#### 3.1.1 Fe@SiO<sub>2</sub>

Fayalite (Fe<sub>2</sub>SiO<sub>4</sub>) for the Fe@SiO<sub>2</sub> catalyst was synthesized. Stoichiometric amounts of Fe (9.13 g), Fe<sub>2</sub>O<sub>3</sub> (26.12 g), and SiO<sub>2</sub> (14.74 g) were weighed out and mixed in a plastic container. The container was filled with argon under a plastic bag to create an inert atmosphere. The powders were ball milled for 30 minutes. The following mixture of powders was then placed in a reactor and heated to 1023 K for 24 hours under argon.

SiO<sub>2</sub> and Fe<sub>2</sub>SiO<sub>4</sub> were mixed in a plastic bottle which was filled with argon under a plastic bag. The mixture was then ball milled for 15 hours. The resulting mixture was fused together at 1873 K for 6 hours in a high temperature furnace. The experimental set up is shown in Figure 15, the sample was placed in an alumina crucible.



*Figure 15: Setup in the high temperature furnace.*

The result from the high temperature furnace was crushed with a mortar, and then leached for 1 hour with nitric acid (0.5 M) during stirring. The leached catalyst was dried at 80 °C for 12 hours.

### 3.1.2 Fe/HZSM-5

The Fe/HZSM-5 (1) catalyst was prepared by the impregnation method described by Guo et al. [4] HZSM-5 (6 g, Zeolyst, 3024E, Si/Al=15) was added while stirring to an iron(III)nitrate solution (5.2 mL, 0.11 M). The iron(III)nitrate solution was prepared by dissolving the appropriate amount Iron(III) nitrate nonahydrate in distilled water to obtain a 0.11 M solution. The catalyst solution was stirred for 12 hours under ambient conditions, followed by 24 hours of stirring at 333 K to evaporate the water content as showed in Figure 16. Afterwards the catalyst was calcined at 823 K for 6 hours. This procedure resulted in a Fe loading of 0.5 %.

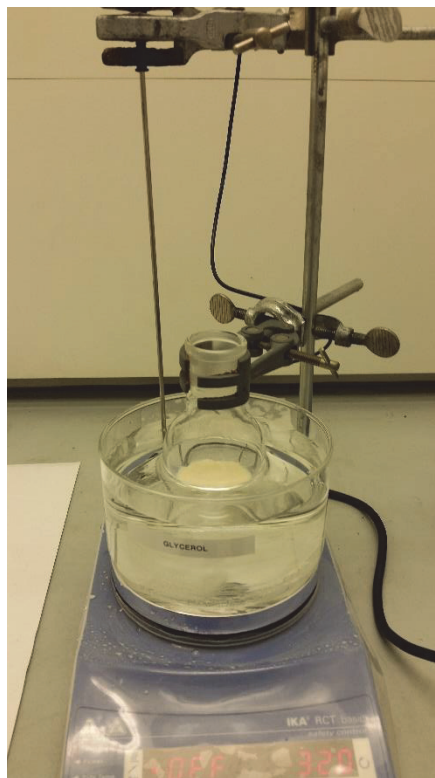


*Figure 16: Catalyst preparation setup.*

A similar catalyst was prepared with a more conventional incipient wetness impregnation method. The same reagents were used, with the only difference being the mixing of the zeolite and iron(III)nitrate solution. The solution was added drop by drop onto the zeolite while continuously stirring. When the sample transitioned into a fluid the addition of solution was stopped. This resulted in a lower volume (2.9 mL) of solution added to what resulted in the catalyst Fe/HZSM-5 (2)

## 3.2 CHARACTERIZATION

### 3.2.1 X-ray diffraction

The synthesized Fayalite was studied with XRD to evaluate the result of the synthesis. A scan with the parameters 15-75 degrees, V6 slit, and a 60 min runtime was performed.

### 3.2.2 N<sub>2</sub>-adsorption

The zeolite and the Fe/HZSM-5 (1) catalyst was characterized by N<sub>2</sub>-adsorption measurements. A sample between 50-100 mg was weighed out and left for degassing at 473 K for at least 12 hours. The tubes with samples were then inserted into the analysis instrument (MICROMERITICS- Tristar II 3020), where the N<sub>2</sub> adsorption curve was measured at 77 K. The specific surface area of the catalyst was calculated by the BET theory, while the t-plot method was employed to calculate the microporous surface area and volume.

### 3.3 ACTIVITY MEASUREMENTS

The non-oxidative conversion of methane was investigated in five experiments, each using a different catalyst or a different temperature program, as shown in Table 1.

*Table 1: The catalysts used for the five activity measurements*

<b>Experiment</b>	<b>Catalyst</b>	<b>Reactor temperature measurement order</b>
1	None	1223 K → 1373 K
2	Fe/HZSM-5 (1)	1223 K → 1373 K
3	Fe/HZSM-5 (1)	1373 K → 1223 K
4	Fe/HZSM-5 (2)	1223 K → 1373 K
5	Fe@SiO <sub>2</sub>	1323 K → 1373 K

The feed ratio was kept constant at 50 volume % nitrogen and 50 volume % methane. The space velocity of the flow differed after which reactor temperature was used as shown in Table 2.

Table 2: An overview of the total space velocity used for each reactor temperature.

Temperature [K]	Space velocity [mL/g·cat·h]
1223	4840
1273	10000
1323	16248
1373	22462

The rig used to measure the activity had flow controllers for regulating the feed flow of methane and nitrogen. The flow controllers were calibrated, and the results are shown in Appendix A. A drawing of the apparatus is shown in Figure 17.

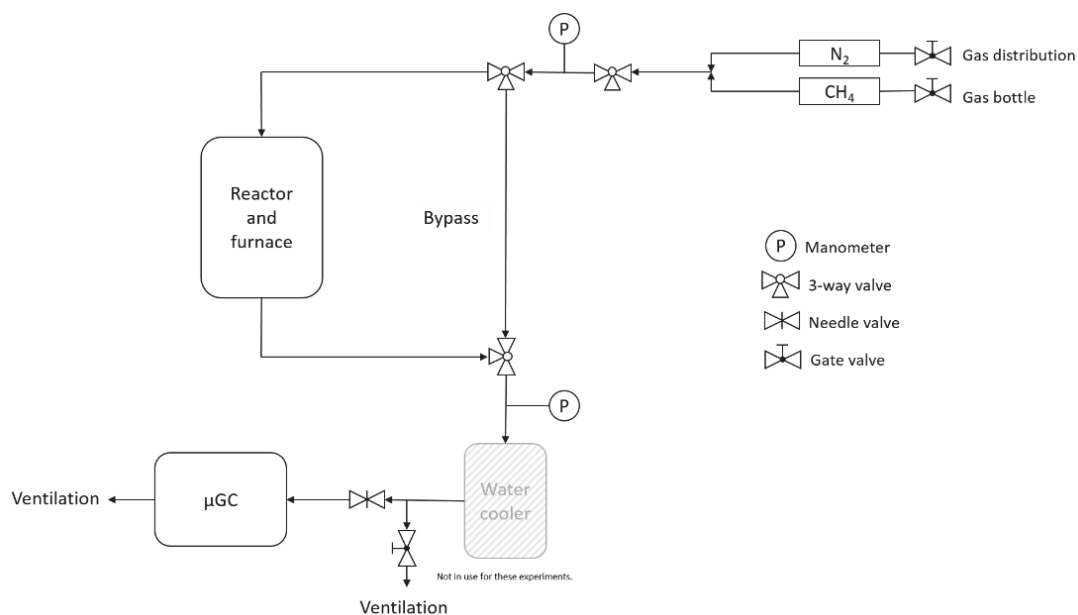
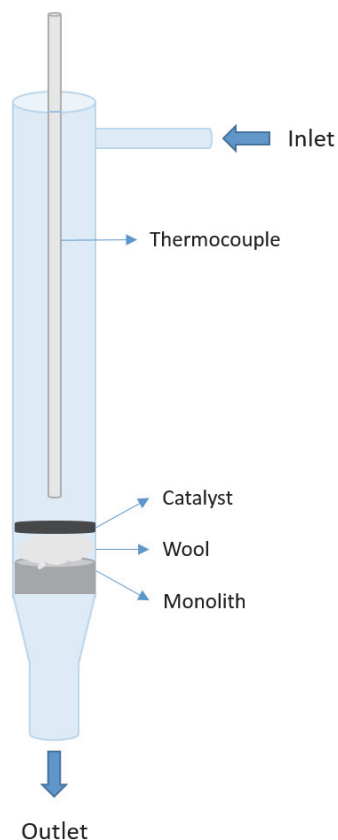


Figure 17: Schematic of the experimental setup involving the reactor used for the activity measurements.

A quartz reactor was used for all experiments, and a drawing of the specifications for the reactor is shown in Figure 18, as well as the catalyst placement for the catalyst. A monolith

with some quartz wool on top was added to the reactor as a base for the catalyst to lie on. The reactor was loaded with 1.0 g catalyst per experiment.



*Figure 18: Schematic of the reactor used for the activity measurements.*

After the catalyst was added to the reactor, the reactor was heated to 1223 K in a pure nitrogen atmosphere before any measurements were performed with the  $\mu$ GC with a heating rate of 10 K/min. When the desired temperature was reached, the flow was adjusted to the predetermined space velocity of methane and nitrogen. The flow was on stream for 5 minutes before the measurements started. For each reactor temperature 3 consecutive measurements were conducted. Each measurement lasted close to 5 minutes. The methane feed was turned off after the last sample was taken. For each reactor temperature the catalyst was in a methane and nitrogen atmosphere for about 15 minutes. As advised by the

projects supervisor, the effluent from four different reactor temperatures (1223, 1273, 1323 and 1373 K) were analyzed.

The table below shows the specifications for the  $\mu$ GC that used to analyze the product stream. The instrument was calibrated with a calibration gas, as well as nitrogen mixed with either ethylene, acetylene or methane. The  $\mu$ GC equations that were obtained are shown in Appendix B.

Table 3: Column types in the Agilent 3000a  $\mu$ GC.

Column	Carrier gas	Components
Molecular sieve, 10 m	Argon	H <sub>2</sub> , O <sub>2</sub> , N <sub>2</sub> , CH <sub>4</sub> , CO
Plot Q, 10 m	Helium	C <sub>2</sub> H <sub>4</sub> , C <sub>2</sub> H <sub>6</sub> , C <sub>3</sub> H <sub>4</sub> , C <sub>3</sub> H <sub>6</sub> , N <sub>2</sub> , CO <sub>2</sub> , CH <sub>4</sub>

### 3.4 ACTIVITY ANALYSIS

A  $\mu$ GC was used to distinguish the product gas stream that came from the reactor. The inlet feed was known due to calibration of the flow controllers, but due to the conversion of methane into hydrogen and other carbon compounds, the volume of the flow changed throughout the process. Nitrogen was used as an internal standard. Nitrogen was inert throughout the whole process, and the nitrogen flow was therefore conserved through the reactor.

By using nitrogen as an internal standard, a dilution factor was derived. The component flow out of the reactor was presumed to be:

$$F_{i,out} = y_{i,out} \cdot F_{tot,out} \quad 3.1$$

$$F_{i,out} = y_{i,out} \cdot Df \cdot F_{tot,out} \quad 3.2$$

Where:

$$F_{tot,in} = \text{Total inlet flow } \left(\frac{m^3}{h}\right)$$

$$F_{i,out} = \text{Outlet flow of component } i \left(\frac{m^3}{h}\right)$$

$y_i$  = Fraction of compound  $i$

$Df$  = Dilution factor

The dilution factor was estimated as demonstrated below:

$$F_{N_2,out} = F_{N_2,in} \quad 3.3$$

$$y_{N_2,out} \cdot F_{tot,out} = y_{N_2,in} \cdot F_{tot,in} \quad 3.4$$

$$F_{tot,out} = \frac{y_{N_2,in}}{y_{N_2,out}} \cdot F_{tot,in} \quad 3.5$$

Where the dilution factor is defined as:

$$Df = \frac{y_{N_2,in}}{y_{N_2,out}} \quad 3.6$$

The conversion of methane was estimated by the following equation:

$$CH_4 \text{ conversion} = \frac{F_{CH_4,in} - F_{CH_4,out}}{F_{CH_4,in}} \cdot 100\% \quad 3.7$$

The carbon based selectivity for ethylene and acetylene was estimated by:

$$Selectivity = \frac{x \cdot F_{C_xH_y}}{F_{CH_4,converted}} \quad 3.8$$

Hydrogen is produced as methane is converted. The hydrogen loss can be a good indication if there is formation of other products than ethane, ethylene and acetylene.

$$H \text{ loss} = \frac{4 \cdot F_{CH_4,in} - (4 \cdot F_{CH_4,out} + 2 \cdot F_{H_2,out} + 6 \cdot F_{C_2H_6} + 4 \cdot F_{C_2H_4} + 2 \cdot F_{C_2H_2})}{4 \cdot F_{CH_4,in}} \quad 3.9$$

## 4 RESULTS AND DISCUSSION

---

### 4.1 CATALYST SYNTHESIS

The article by Guo et al. [4] did not mention how the fayalite was obtained, or whether it was synthesized or not. Due to the difficulty of obtaining the naturally occurring mineral, it was decided to synthesize it from iron, iron oxides and silica. Several synthesis methods were found in the literature, and in the end one was based on its simplicity, as well as the fact that the equipment needed to performed the synthesis was readily available. The synthesis was performed as described in the article by D. Daval et al. [11] There was, however, a discrepancy when it came to ball milling the mixture in argon. Due to the need for an urgent synthesis, and lack of equipment, the container used for ball milling was filled with argon using a somewhat easy solution. It is plausible to think that this method did not manage to fill the container with a completely pure argon atmosphere, resulting in an unknown amount of oxygen present during ball milling. This could have an effect on the composition, especially for the iron that could potentially have been oxidized.

The fayalite was characterized by XRD, and the peaks obtained are shown in Figure 19. As shown in the figure, there is an overlay of the peaks that occur for pure fayalite. The disturbance in the area 5-30 degrees indicate that the sample contains amorphous species. The overlay shows that there is an overlap between the two plots, but that there is some significant deviance.

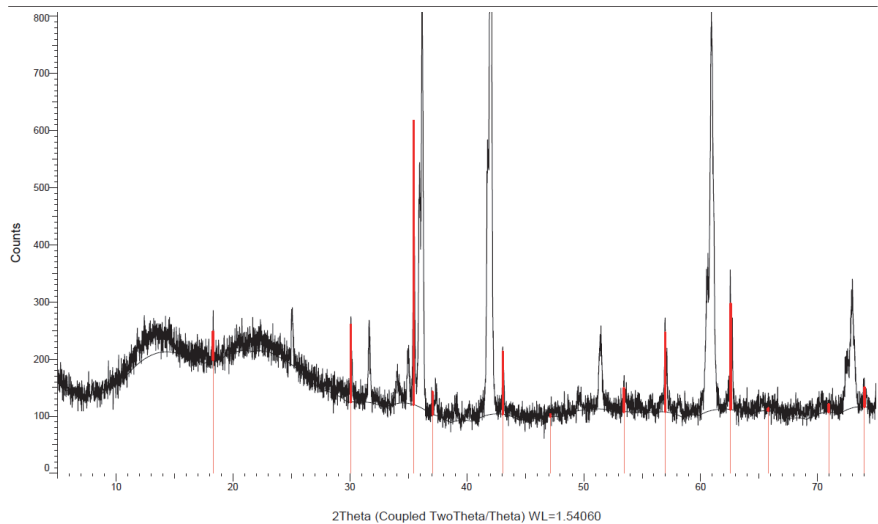


Figure 19: XRD plot for the synthesized fayalite with an overlay of pure fayalite.

The obtained peaks were also compared to an overlay of FeO in Figure 20. The overlay shows clearly that it is likely that there is some FeO in the sample, seeing as the peaks that were missing from the fayalite plot is identified here.

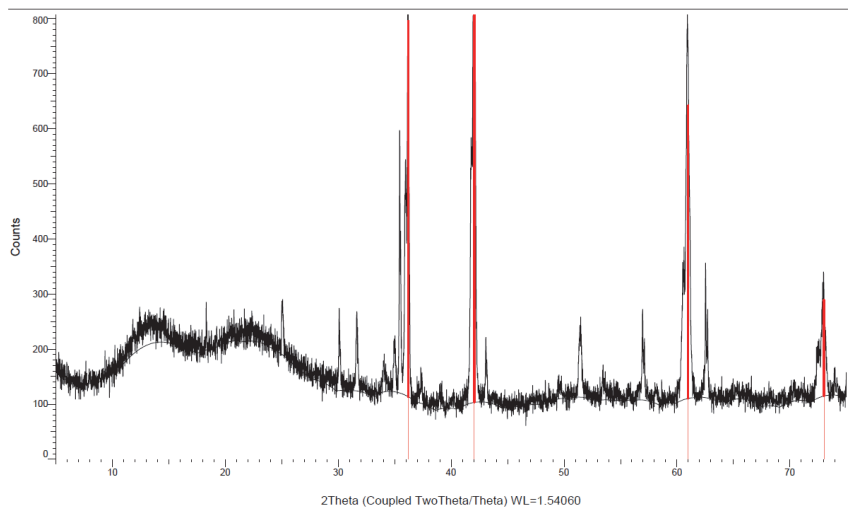


Figure 20: XRD plot of the synthesized fayalite with an overlay of FeO.

The XRD plot indicate that some fayalite was indeed produced, but that there also was a presence of FeO. Seeing as the synthesized material was not pure fayalite, it should be taken

into consideration that the starting materials for the catalyst preparation was not ideal. And it may be that that this could have had an influence on the catalyst and its activity.

#### 4.1.1 Fe@SiO<sub>2</sub>

The catalyst was prepared as close as possible according to the instructions from Guo et al. [4] The synthesized fayalite and silica were weighed out in the proportions given in the article. The powders were mixed together, and ball milled thoroughly. The same difficulty with providing a pure argon atmosphere arose here as for the synthesis of fayalite. The ball milling called for a pure argon atmosphere, but due to the lack of necessary equipment it was decided to use the same method of introducing argon inside a plastic bag to be able to move forward with the catalyst preparation.

The next step was to fuse the mixture together at 1973 K. To reach such a high temperature an induction furnace was approached. However, this method did not work for the powder mixture. The sample was not activated by the induction field, and the powders never increased in temperature. Usually this sort of technique is performed with solid iron on top of the powder mixture, which can be activated by the induction field, and kick of the temperature increase for all the reagents. This was considered as a possible way of introducing deviations in composition. Together with the metallurgist responsible for the induction furnace it was decided that this furnace was not a suitable choice. Due to these results a second high-temperature furnace was sought out. Unfortunately, no furnace was found that could sustain temperatures up to 1973 K. However, a furnace that could reach a temperature of 1873 K, belonging to the Department of Materials Science and Engineering, was found and ultimately chosen as the furnace to be used for the catalyst mixture. The furnace gave the right atmosphere, as well as the constant temperature over the course of the six hours that was required. It is unknown how large the effect the lowered temperature would have on the finished catalyst, but it is important to keep in mind the deviations from the original procedure when comparing the catalyst activity results. A drawback when using this furnace was the low amount of catalyst mixture it could handle. Only an amount

necessary for one experiment could be produced at a time. Figure 21 shows the immediate result from the high temperature treatment. As can be seen from the picture the mixture has fused together to a solid, and there is a white crust around it. The inside of the solid is brown. The solid was crushed in a mortar. From this visual result shown in the figure it is likely to believe that the catalyst was not homogeneous, and the properties of the layer on top of the solid might differ from those inside. Guo et al. [4] did not mention if there was used a specific particle size of the catalyst, so this was not emphasized in this project.



*Figure 21: The result from fusing together the powders in the high temperature furnace.*

After the mixture was fused together it was leached with nitric acid. Guo et al. [4] only mentioned the molarity of the leaching agent, but did not offer any further details on how the procedure was accomplished. This lack of information leads to an uncertainty in the procedure, which adds an uncertainty to the result of the catalyst. The leached catalyst was dried according to the procedure listed in the article.

#### 4.1.2 Fe/HZSM-5

The Fe/HZSM-5 (1) catalyst was prepared after the instruction given by Guo et al. [4] The same type zeolite (zeolitt 3024E) was used to obtain a catalyst with similar characteristics. After stirring first at room temperature and then at 333 K, the mixture had the appearance shown in Figure 22. The mixture had dried out in the bottom of the round-bottom flask, and a pattern appeared in the material. Some parts of the mixture had a clear yellow tint, which may be due to an uneven dispersion of the iron(III)nitrate solution on the zeolite material.



*Figure 22: Fe/HZSM-5 catalyst mixture”.*

When the mixture was removed from the flask, a further unevenness in color was noticed. The inside of the mixture was clearly lighter in color and more white than the surface. If the color of the solid is an indication of the distribution of the iron solution, it is likely to think that the prepared catalyst was not a homogeneous blend. An uneven loading of iron on the catalyst particle would add an uncertainty to the measurements, and possibly affect the activity and selectivity of the catalyst.



*Figure 23: Catalyst before crushing with mortar.*

The Fe/HZSM-5 (2) catalyst delivered the same results during stirring. After crushing both catalyst blends with a mortar they were both calcined at 823 K.

The volume of iron(III)nitrate solution added to the zeolites for the two catalysts differed, which also would affect the Fe loading. The volume added to the Fe/HZSM-5 (2) catalyst was significantly lower, in fact only 56 % of the volume prescribed by Guo et al. [4] was added. This would lead to a lower Fe loading on the catalyst.

## 4.2 CATALYST CHARACTERIZATION

The Fe/HZSM-5 (1) catalyst prepared by the preparation method given by Guo et al. [4] was characterized by N<sub>2</sub>-adsorption. The results that were obtained by the measurements are shown in Table 4. When comparing these results to the findings by Tan [14] one discrepancy becomes apparent. When the zeolite was loaded with Fe the BET surface did not decrease, but rather the opposite. All the values are based on three parallel measurements, which all followed the same pattern of a lower BET area for the untreated zeolite. Despite this

deviance, the other results obtained displayed a correlation to what was proclaimed by Tan. [14] The microporous area and volume both decreased when the catalyst had its Fe loading increased from 0 to 0.5 %, while the external surface area increased. This supports the theory in which Fe does not block the zeolite channels, but rather migrates into the zeolite pores. The pore size also increased with iron loading.

However, these measurements were only performed for one amount of Fe loading, and not repeated for different amounts of active material. Hence it was not confirmed that further Fe loading would lead to even further loss of microporous surface and volume, or increase in external surface area. The Fe loading in the project was also relatively low compared to the amount of Fe in the catalysts prepared by Tan. [14] The difference in the values obtained from untreated zeolite and loaded catalyst was quite prominent compared to the low amount of Fe loading. The results presented by Tan [14] did not reflect that the Fe loading had the same striking impact on the measurement results. However, the preparation methods were not identical and there was also a difference in the type of zeolite used between the two projects.

With all of this in mind, these measurements were considered to indicate that the zeolite was successfully impregnated with Fe.

*Table 4: N<sub>2</sub>-adsorption results*

<b>Fe loading (wt %)</b>	<b>S<sub>BET</sub> (m<sup>2</sup>/g)</b>	<b>S<sub>micropore</sub> (m<sup>2</sup>/g)</b>	<b>S<sub>external</sub> (m<sup>2</sup>/g)</b>	<b>V<sub>micropore</sub> (cm<sup>3</sup>/g)</b>	<b>Pore size (Å)</b>
0.0	359	278	75	0.13	25
0.5	379	243	133	0.11	26

Notes: S= surface area, V=volume

### 4.3 REACTION SET-UP

Preliminary experiments were carried out to evaluate the reactor set up, to ascertain the suitability of the equipment. The ratio between methane and nitrogen was different than that which Guo et al. [4] used. It was decided to use a feed consisting of mainly nitrogen and a smaller portion of methane. This was done to minimize the coking in the reactor. The initial results showed an inconsistency in the methane conversion obtained at different temperatures. The space velocity was also different; it was kept high because of limitations in the equipment.

It was expected that the conversion would increase with increasing temperature. Though this was partly true, it also revealed a systematic pattern in the conversion. The conversion would go up and down, while at the same time slowly increasing during the temperature increase. Since the flow was kept constant, it could suggest that something regarding the temperature control was incorrect. The temperature controller could not be programmed and the temperature had to be manually increased, which also added an element of inconsistency to the experiment.

The feeding of methane was also found to be insufficiently accurate. The methane flow was unstable, and the amount detected by the  $\mu$ GC was larger than what was presumed to be fed to the reactor. There was also an issue with separating the product flow. The reactor was at a temperature where it would be expected to obtain acetylene as well as ethylene, but the resulting  $\mu$ GC plots could not confirm this.

With these preliminary results in mind, several alterations were performed to the reaction set up. A new temperature controller (Eurotherm 2416P4) was installed, to obtain better control and a consistency in heating of the reactor. The flow controller for methane was replaced with a model that could accommodate a lower flow, which made it possible to use a total space velocity equal to that of Guo et al. [4] A new methane gas bottle was also installed, to further ensure a stable methane feed. Another modification to the reactor set up was the installation of a rotameter to ensure a reliable flow of the reactor effluent to the

$\mu$ GC.

Ethylene and acetylene was co-fed to the  $\mu$ GC to investigate if their respective peaks could be identified, however only one peak was observed. This confirmed that during the initial testing of the reactor there could have been acetylene formation, but that the column did not separate the compounds. However, the literature[23] confirmed that the PLOT q column could separate acetylene, ethylene and ethane. Therefore, several settings were adjusted while observing the results, to see if two peaks could be obtained. By lowering the temperature from 60 to 42 °C, and the pressure from 35 psig to 25 psig, the two compounds could confidently be separated. A more in-depth description of the separation of acetylene and ethylene can be found in Appendix C.

Lastly, the  $\mu$ GC was calibrated using the new settings. The different gases were fed to the  $\mu$ GC by the use of a gas mixer, GasMix™. By using the GasMix the calibration gas could be diluted, which made it possible to analyze the different gases at several feed percentages, which would increase the accuracy of the  $\mu$ GC equations.

#### 4.4 CATALYST ACTIVITY

The activity measurements were performed similarly to the experiments performed by Guo et al. [4] Regarding the space velocity, it was not mentioned whether it was the methane space velocity or the total velocity that was reported. For these measurements it was considered to be the total space velocity of both nitrogen and methane. All experiments used the same total space velocity as Guo et al. [4], increasing the space velocity as the temperature was increased in the reactor. However, the composition of the feed was different. The installation of the new flow controller allowed for a smaller feed of methane than to begin with, but to be able to use the same total space velocity the composition of nitrogen and methane was chosen to be 50:50. This decision was made under advisement from the projects supervisor. The low ratio of methane in the feed could have an effect on the results, but it is unknown to what extent. Having a similar space velocity as Guo et al. [4] was an important component of obtaining comparable results. The longer retention time the

gas experiences in the reactor, the longer time the components have to react. This is important for the formation of coke. Acetylene will eventually with enough time dehydrogenate to coke. Therefore, to be able to accurately compare the results, it was important to us the same space velocity as Guo et al. [4] At every temperature the measurements three consecutive samples were taken to ascertain that there was a continuity in the results. The methane flow was turned off when heating the reactor for the next temperature level to avoid unnecessary coking of the reactor.

The analysis of the data from the  $\mu$ GC was based on using nitrogen as an internal standard. The area of the inlet used to determine the dilution factor was based on measurements conducted at ambient conditions. With the new flow controller, the methane flow had a greater stability, and there was no issue with the  $\mu$ GC detecting a larger amount of methane in the product flow than was fed to the reactor.

The empty reactor experiment and the two zeolite catalysts were measured from 1223 K and upwards, while the measurements using the Fe@SiO<sub>2</sub> catalyst started at 1323 K under advisement from the projects supervisor. The intention was to cool the reactor down so measurements could be completed at the two remaining temperatures. During the measurements at 1373 K there was pressure buildup, indicating heavy coke formation. The measurements for this catalyst were therefore only performed at 1323 and 1373 K.

The methane conversion obtained with the synthesized catalysts and the blank experiments is illustrated in Figure 24. The obtained results confirm that with increased temperature the conversion of methane also increases. For the lower temperatures there can be seen a significant difference in conversion between the empty reactor experiment, and the two experiments with the Fe/HZSM-5 catalysts. This indicates that the iron catalyst is active at the temperatures 1223 and 1273 K, and contributes to the conversion of methane. The conversion obtained at 1273 K with the Fe/HZSM-5 (1) catalyst was larger than the conversion obtained at 1223 K. According to theory, the methane conversion should decrease with increasing temperature. From the results obtained for the Fe/HZSM-5 (2) catalyst, a small

drop in conversion between 1223 and 1273 K can also be seen. This result could therefore indicate an inaccurate analysis of the product stream. The fluctuating conversion during the preliminary experiments was larger than what was observed in these measurements, and these measurements were not deemed to indicate any issues with the temperature control.

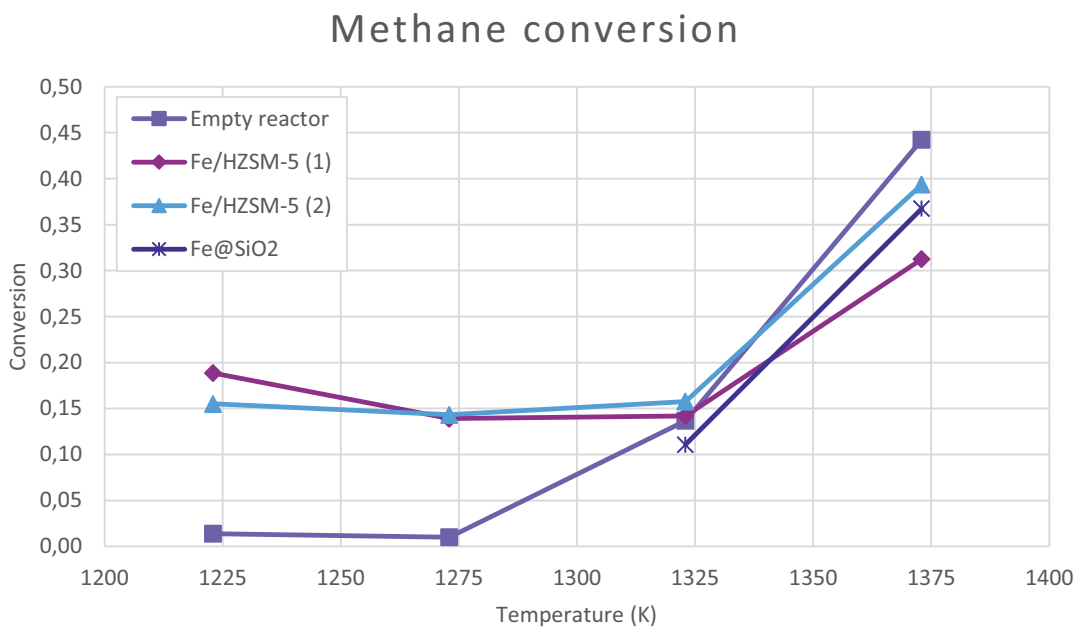


Figure 24: The methane conversion obtained with the prepared catalysts and empty reactor experiments.

When the reactor temperature reached 1323 K the empty reactor achieved a conversion that was similar to the catalyst driven experiments. At the highest reactor temperature, 1373 K, all four experiments experienced a large increase in methane conversion. This could indicate that as the temperature increases the gas phase reactions are dominating, and a maximum conversion is obtained.

Guo et al. [4] reported a conversion of 48 % at the highest temperature, 1363 K. The empty reactor experiment reached the most similar conversion, i.e. 45 %. In the other experiments there was also a large spike in conversion when reaching 1373 K, varying from 30 to 40 % conversion. Between the two Fe/HZSM-5 catalysts there was a difference of almost 10 % for the maximum conversion. However, when running the experiment at the highest

temperature for all catalysts there was a pressure buildup in the reactor. The pressure buildup most likely occurred from coking in the reactor. Coke deposition on the catalyst would lead to difficulty of the gas stream passing through the reactor, and it cannot be certain that the gas leaving the reactor was an accurate representation of the products obtained. Therefore, there is an uncertainty over the measurements performed at 1373 K.

The hydrogen production can be viewed as a good indicator of the methane conversion. Figure 25 shows the estimated hydrogen flows obtained during the different experiments. The similarities between the two zeolite supported catalysts appear clearly, supporting the theory that they behave similarly, and that the synthesis method did not produce significantly different catalysts. The difference in Fe loading on the zeolite did not seem to have a significant effect on the catalysts activity.

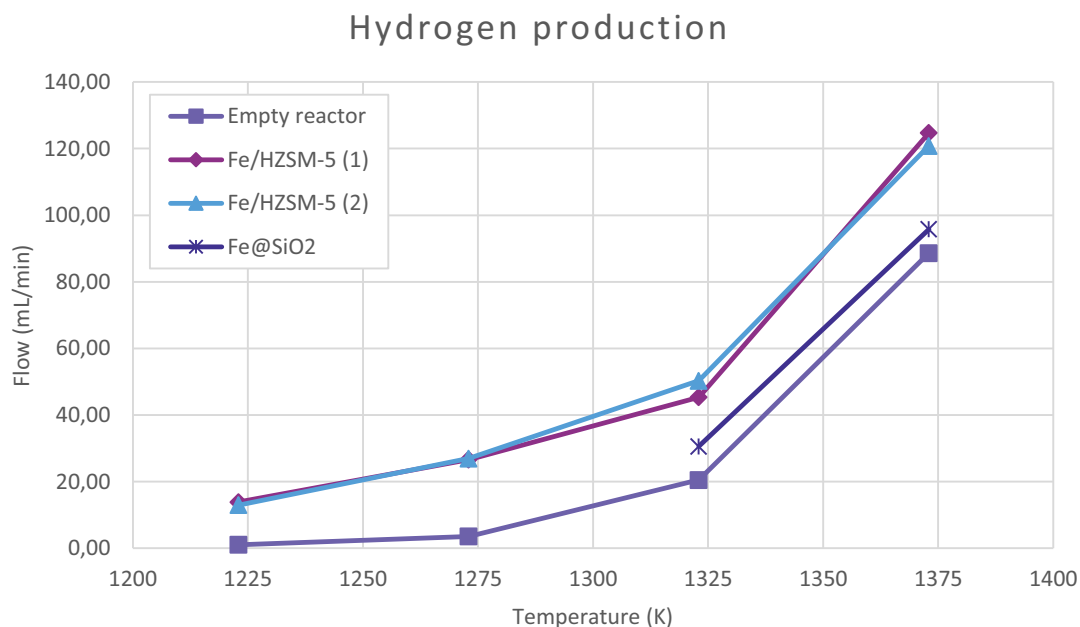


Figure 25: Hydrogen flow in product stream.

The hydrogen produced during the empty reactor experiment further indicates that there is low conversion at the two lowest temperatures. When the temperature is increased to 1323 K the hydrogen production increases and reaches its peak at 1373 K. The hydrogen production obtained while using the Fe@SiO<sub>2</sub> catalyst and no catalyst at all is very similar. The hydrogen production from these two experiments is noticeably lower than the hydrogen obtained by using iron impregnated on zeolite as a catalyst.

The low hydrogen production could be attributed to the formation of higher hydrocarbons, such as naphthalene and benzene. By inspection of the reactor after the experiments, the Fe@SiO<sub>2</sub> catalyst and monolith was completely black as shown in the picture below (Figure 26). All the catalysts were blackened by carbon, but there was one noticeable difference on the spent Fe@SiO<sub>2</sub> catalyst. The residue was oily compared to the residue from the other experiments, which is consistent with the production of higher hydrocarbons.



Figure 26: Fe@SiO<sub>2</sub> catalyst and monolith after the experiments.

The reactor design used during the experiment contained a large free space above and after the catalyst where the gas flow is heated up. In the open volume space the gas phase reactions will be free to dominate without an impact from the catalyst. By examination of the schematic of the reactor used by Guo et al. [4] it becomes clear that the reactor also contained this free space. Even though it is reported that at high temperature there is no acetylene formation, the free space in the reactor is not discussed. The catalyst is claimed to “*suppress complete dehydrogenation*”, which would account for the absence of formation of acetylene on the catalyst. But aside from these claims, there is a part of the reactor that is heated where the gas flow will not be in contact with the catalyst. How the catalyst can inhibit gas phase reactions is not revealed, and is a point of interest for future research. In the free space where the gas is heated up there will, according to the equations for methane pyrolysis, be formation of acetylene. Previous experiments [3] with thermal pyrolysis have all shown that acetylene should be an important product. The formation of ethane is usually low due

to thermal pyrolysis. Provided that the analysis of the product stream by Guo et al. [4] is correct, it could be that the Fe is an effective catalyst for hydrogenating acetylene. However, this does not account for free volume after the catalyst where the gas stream will still be heated and not come in any further contact with the catalyst. A possibility to reduce the gas phase reactions is to redesign the reactor, ensuring a low free space volume where gas phase reactions can occur. Limiting the amount of heated free volume would inhibit the impact of thermal pyrolysis on the products obtained in this process.

Guo et al. [4] reported its product distribution at 1223 K (see Figure 9), and Figure 27 shows the product distribution of the experiments performed in this project. Comparison of the products obtained during the blank experiment performed by Guo et al. [4] and the results from the empty reactor experiment in this project showed distinct similarities. The main product from both experiments was coke. It is important to note that the analysis instrument used in this project did not have the ability to detect higher hydrocarbons, meaning there is a potential for other compounds in the product fraction labeled coke. The fraction of coke formed in this project was lower (87 % versus 95 %) and the conversion was also lower (1 % versus 2.5 % for Guo et al. [4]), but they are still counted as similarities. Moreover, the similarities between the product distribution of ethane and ethylene is also apparent from these results. The main hydrocarbon product is ethylene, but there is also a slight formation of ethane. The main difference when comparing these two results is the formation of acetylene in this project. Even at this low temperature a small portion of acetylene is formed. In the experiments performed by Guo et al. [4] there is no mention of acetylene formation.

The principal product for the two iron impregnated zeolites was also coke. However, the same catalyst used by Guo et al. [4] produced large amounts of naphthalene and benzene. Since there was no analysis done on the residue and the  $\mu$ GC could not separate higher hydrocarbons it cannot be excluded that naphthalene or benzene was produced. Apart from the formation of acetylene, it cannot be confirmed that the coke formation, by itself, directly contradict the results obtained by Guo et al, since the amount of benzene and naphthalene

are unknown. A more in depth analysis of the product gas stream would be a prudent next step to confirm whether it contains higher hydrocarbons or not.

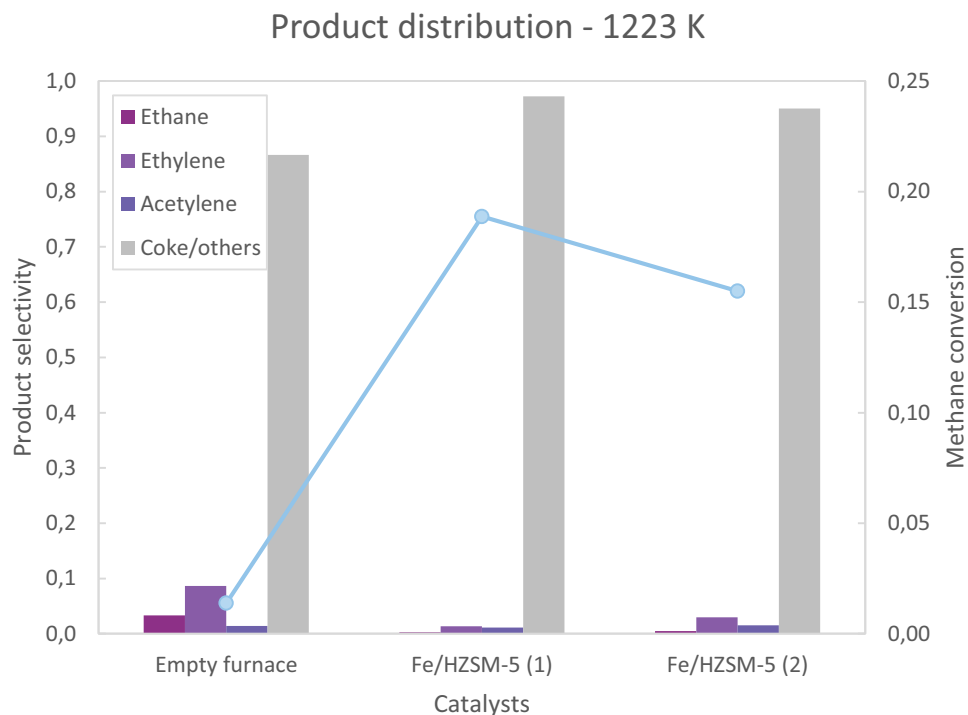


Figure 27: product distribution at 1223 K. The associated methane conversion level is displayed linearly in the diagram.

A comparative diagram of the product distribution at 1323 K was also performed, enabling the results obtained by the Fe@SiO<sub>2</sub> catalyst to also be analyzed. These results are presented in Figure 28. Guo et al. [4] did not perform any experiments at this temperature, but the results show that by using the Fe@SiO<sub>2</sub> catalyst both below and above 1323 K, the obtained product stream had a >99 % selectivity towards hydrocarbons. However, in this project it was apparent that coke was a product just by visual inspection of the reactor and the spent catalyst. As shown in Figure 26 the catalyst was pitch black after the experiment, and Figure 29 shows that the reactor also became covered in coke. The reactor was visually inspected after every experiments, and the results were unanimous, the reactor was always covered in a black substance.

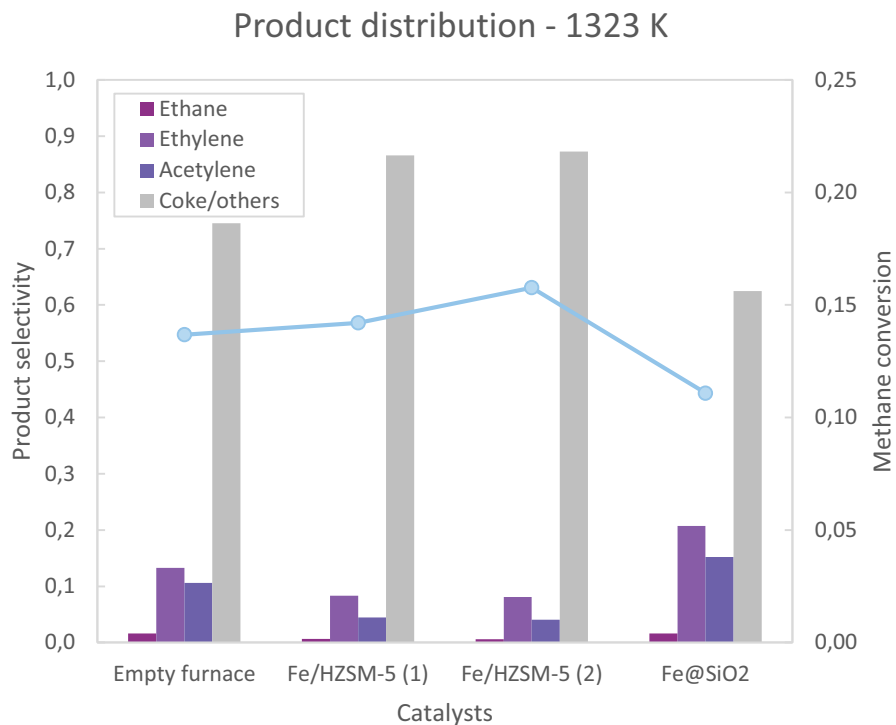


Figure 28: Product distribution at 1323 K for the 3 different catalysts. The associated methane conversion level is displayed linearly in the diagram.

In accordance with Guo et al. [4], the Fe@SiO<sub>2</sub> catalyst achieved the most desirable product composition. It produced the least amount of coke, and the largest amount of ethylene. At a methane conversion of 11 % a selectivity towards ethylene of 21 % was obtained. The closest reactor temperature Guo et al. [4] presented results for was 1303 K. At 1303 K the conversion was 42 %, and the carbon based selectivity towards ethylene, benzene and naphthalene were roughly 40, 22 and 38 % (taken from Figure 3). The results obtained in this project by the Fe@SiO<sub>2</sub> catalyst were not in the same range as those by Guo et al. [4] But that could be attributed to the deviances in the catalyst preparation. Though the selectivity to benzene and naphthalene cannot be substantiated from these results, the hydrogen flow can give an indication if there was formation of higher hydrocarbons. The experiments with the empty reactor and the two zeolite catalysts both obtained a similar methane conversion at 1323 K. Figure 25 showed that the hydrogen production obtained with the two zeolite catalysts were substantially higher than for the empty reactor experiment. This indicates that there was a

lower amount of hydrocarbons formed when using the Fe/HZSM-5 catalysts, and a larger portion of coke. This is also reflected in the product distribution where the amount of coke produced is highest for the two zeolite catalysts. The Fe@SiO<sub>2</sub> catalyst obtained a lower conversion of methane at 1323 K, and therefore it is not possible to relate its hydrogen production to a higher or lower hydrocarbon formation than obtained by the zeolite catalysts. What is clear from these results is that the product distribution deserves a more thorough investigation, and that the results obtained by the Fe@SiO<sub>2</sub> catalysts is promising.

Another contradiction to Guo et al. [4] became apparent when looking at the amount of acetylene formed. At 1323 K the product streams for all experiments produced a significant amount of acetylene.

The ethane formation remained low for all experiments. This does not support the findings reported by Guo et al. [4] The DFT calculations predicted that the conversion of ethane to ethylene happened rapidly, which was the reason that no ethane showed up during their measurements. But for all measurements, there was a low amount of ethane formation. That includes the measurements performed with the Fe@SiO<sub>2</sub> catalyst.

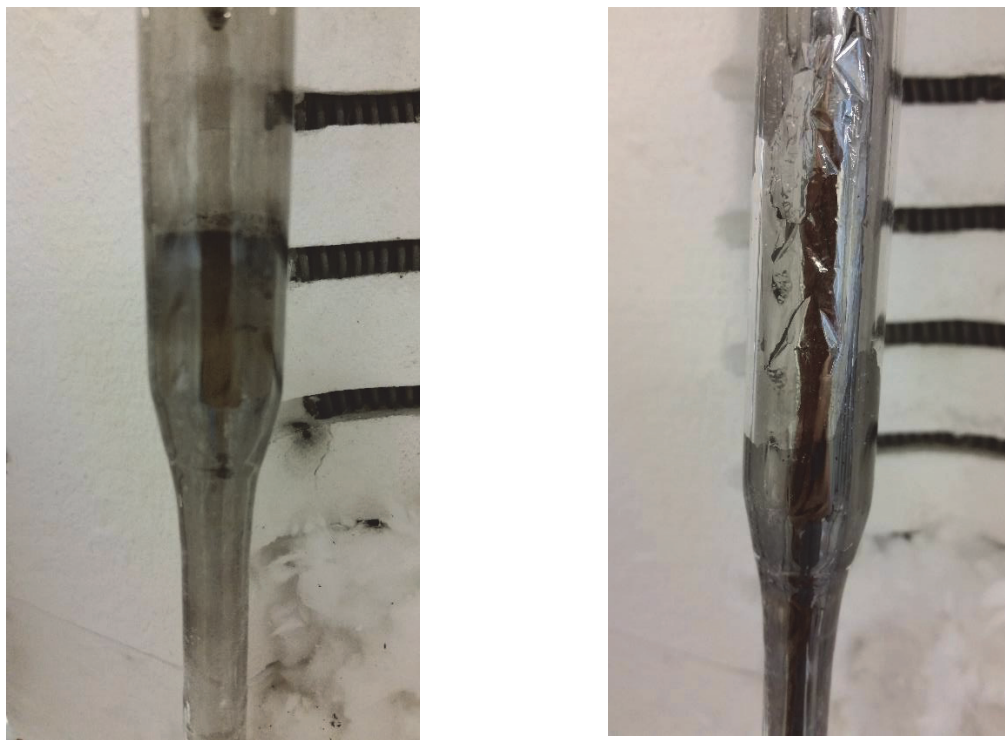


*Figure 29: Reactor before and after.*

Even though benzene and naphthalene could not be detected by the analysis instrument, the mass balance of hydrogen could be estimated to confirm or disprove the formation of higher hydrocarbons. If there was any substantial deviance loss in hydrogen, it could indicate that higher hydrocarbons had been formed. A diagram showing the hydrogen loss is shown in Figure 30. The hydrogen loss at 1223 K is centered around 0 %, which indicates that there is no or little formation higher hydrocarbons. For the two following temperatures the hydrogen loss is less than 0 % for the two Fe/HZSM-5 catalysts. A negative hydrogen loss means that there is more hydrogen leaving the reactor than what is fed in, which is not possible. These calculations show that the precision in the analysis is lacking. However, the results can be used as an indication of the hydrogen loss. The hydrogen loss reaches 5% at 1323 K, and over 18 % for the blank experiment at 1373 K. Though the exact hydrogen loss is uncertain, this extensive amount is a good indication that there is formation of higher hydrocarbons, possibly benzene and naphthalene. The formation of coke does not contribute to the hydrogen loss, since the hydrogen in methane would be stepwise released as shown in

equation 1.1 and measured as hydrogen by the  $\mu$ GC. The Fe@SiO<sub>2</sub> and Fe/HZSM-5 (2) catalyst experiments experience the same rise in hydrogen loss at 1373 K, indicating formation of higher hydrocarbons. Measurements from Fe/HZSM-5 (2) deviate from the trend, and remains negative in the hydrogen loss throughout all the measurements above 1223 K. However, as noted earlier this experiment experienced a pressure buildup, leading to an uncertainty in the result.

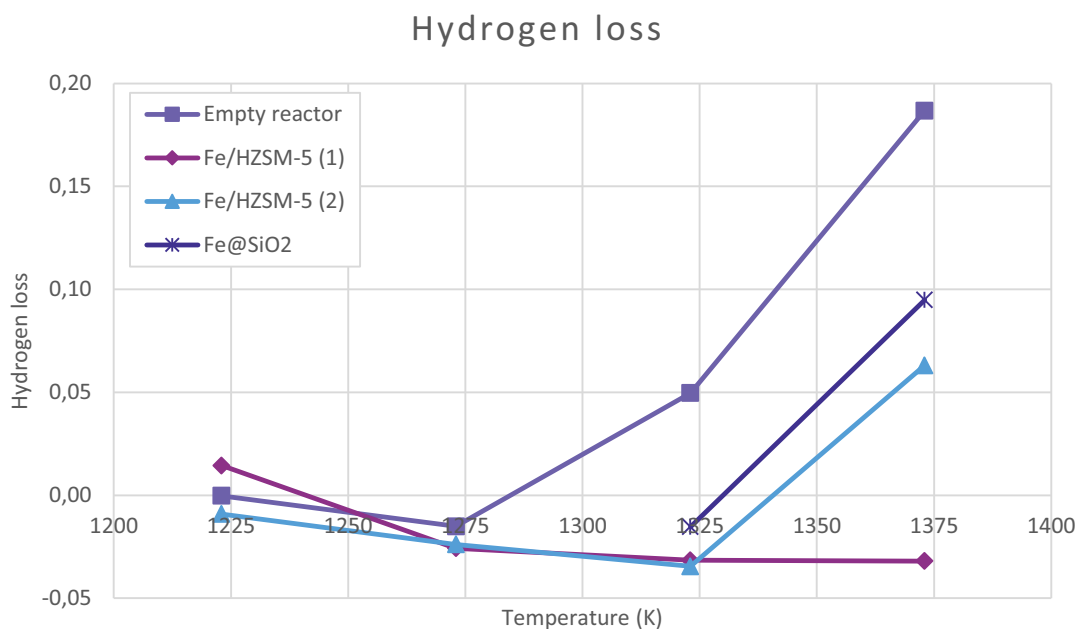


Figure 30: The estimated hydrogen loss for the four experiments.

The selectivity towards ethylene and acetylene was compared in Figure 31 and Figure 32. The ethylene selectivity decreases as the reactor temperature increases. The highest selectivity towards ethylene is achieved at 1323 K while using the Fe@SiO<sub>2</sub> catalyst, however from Figure 32 it can be seen that the acetylene selectivity is also high at this temperature. When the reactor temperature is increased to 1373 K both selectivities are lowered, which is also similar for the empty reactor measurements. For the two Fe/HZSM-5 catalysts the ethylene selectivity has its peak at 1323 K, moreover the ethylene selectivity is similar across all

temperatures. The selectivity for acetylene, however, differ when the temperature rises to 1373 K.

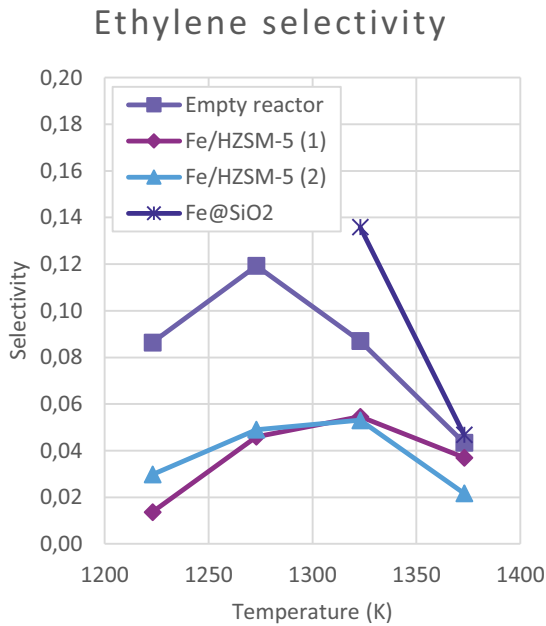


Figure 31: Ethylene selectivity obtained for the four experiments.

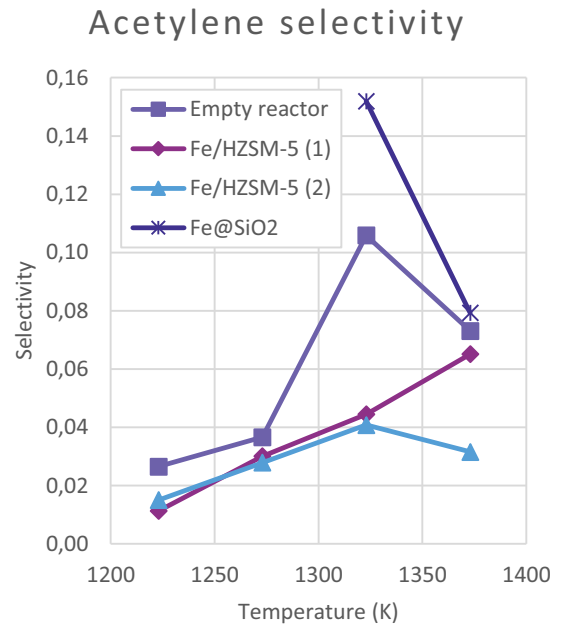


Figure 32: Acetylene selectivity obtained for the four experiments.

The selectivity towards ethylene obtained by Guo et al. [4] fluctuated for the reactor temperatures that were examined. As seen in Figure 3 the selectivity reached its peak at 1273 K. This is quite similar to the results that were obtained in this project. There was not conducted measurements at enough reactor temperatures to confirm the fluctuation of the ethylene selectivity.

A different perspective on the selectivity towards ethylene is shown in Figure 33. The ethane selectivity was plotted against the conversion obtained at each temperature. Each point on the diagram represents one temperature, starting from 1223 K up to 1373 K. The first selectivity estimated at 1223 K for the three experiments conducted at this temperature is

noticeably lower than the following selectivities estimated at the higher reactor temperatures, 1273 and 1323 K. It appears that the selectivity for each measurement reaches its peak at the reactor temperature of 1273/1323 K, regardless of the different conversion obtained. Nonetheless, despite the difference in selectivity and conversion across all four experiments, a trend is observed as the reactor temperature increased to 1373 K, thus increasing the methane conversion. As the methane conversion increased, the selectivity towards ethylene steadily decreased.

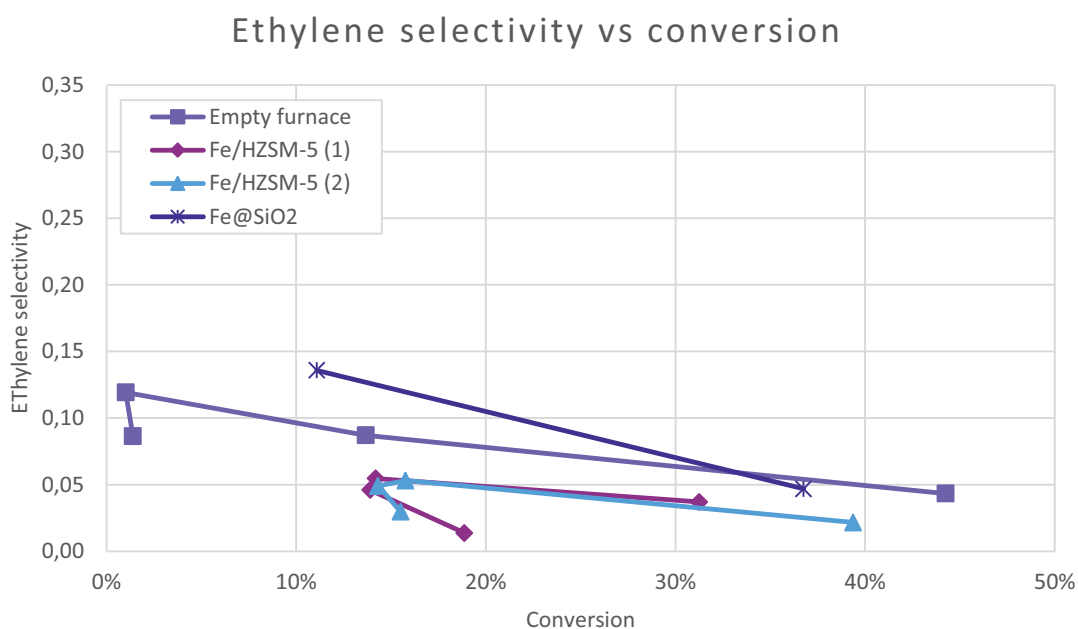


Figure 33: Selectivity vs conversion

As demonstrated by the hydrogen mass balance, the accuracy in the analysis, specifically the  $\mu\text{GC}$  equation obtained from the calibration of the hydrogen was lacking. The carbon based selectivity is based on both the equations for methane, as well as the equations for ethylene and acetylene. Basing all the results on these equations might lead to a misinterpretation of the selectivities. At least there is an uncertainty in the results. To circumvent the uncertainty from the calibrations, the  $\mu\text{GC}$  response area from the  $\mu\text{GC}$  was compared directly. Figure 34 shows the corresponding ratio between the ethylene and acetylene area at each reactor

temperature. The diagram shows that as the reactor temperature increases the ratio between ethylene and acetylene lowers, meaning that at higher temperatures the acetylene production increases in comparison to the ethylene production. The higher acetylene production at high temperatures is as expected. Most importantly what can be derived from this diagram is that the relationship between the two products is similar at high temperature, and the addition of a catalyst did not have any impact on the ratio between ethylene and acetylene at the 1373 K.

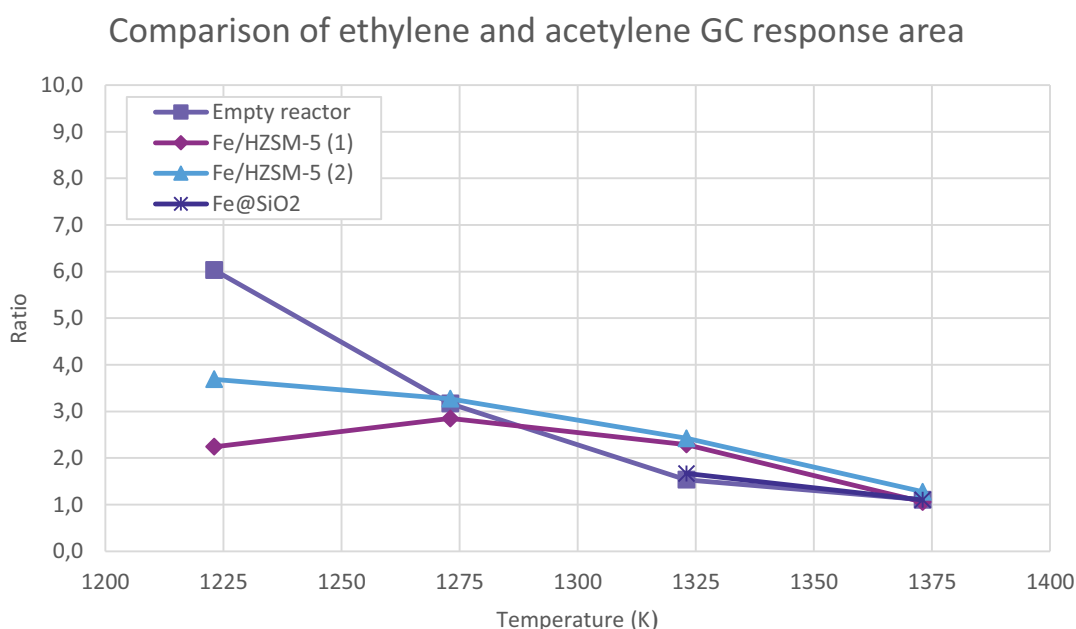
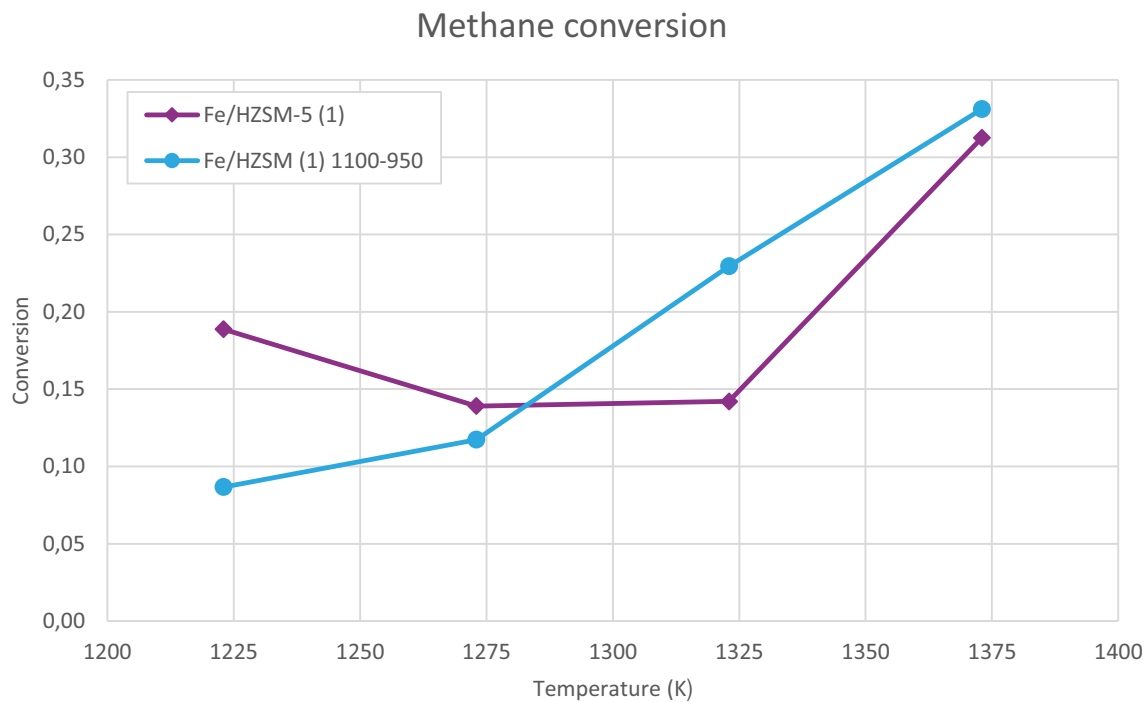


Figure 34: The response area for ethylene and acetylene is compared in the figure.

The experiment with the Fe/HZSM-5 (1) catalyst was repeated to examine if there was any significant deactivation of the catalyst during the previous experiment. By heating the reactor to the highest temperature, 1373, immediately and conducting the first measurement at this temperature the methane conversion could be compared. During the first experiment the catalyst had already been on stream with a feed consisting of methane and nitrogen for around 45 minutes (15 minutes per reactor temperature) when the reactor reached 1373 K. It is likely that any coking would have already occurred during this time period that could

have affected the conversion. As demonstrated in Figure 35 the conversion at 1373 K is slightly higher for the unused catalyst. The difference is, however, quite minimal, and it is not considered to confirm any deactivation. There are two areas on the diagram that stands out in terms of deactivation. After the measurement at 1373 K, the temperature was lowered down to 1323, 1273, and finally 1223 K. At 1323 K the difference in methane conversion was 9 %. At the highest temperature the space velocity of methane was highest, which makes it reasonable that there would be a more significant amount of coking on the catalyst, than at lower temperatures that employed lower methane space velocities. The conversion was quite similar when the reactor temperature was 1273 K, but when the reactor temperature was lowered even further to 1223 K the conversion yet again differed with a 10 %. The experiment using the fresh catalyst obtained a conversion of 19 %, while the spent catalyst that had been on stream for roughly 45 minutes only obtained a conversion of 9 %. These results indicate that the catalyst is prone to deactivation, with the temperatures 1223 and 1323 K being particularly interesting for further research into the deactivation of the catalyst. However, it is possible that the catalyst is inhomogeneous, and thus will deliver different results depending on which part of the sample is loaded into the reactor. The visual inspection of the prepared catalyst showed a large variety, which could be attributed to different Fe loading on the zeolite particles. Considering the results from the catalyst preparation this is considered a plausible explanation.



*Figure 35: The Fe/HZSM-5 catalyst methane conversion analyzed from low temperature to high, and opposite.*

The second set of measurements with the Fe/HZSM-5(1) catalysts also serves to show the reproducibility of the conducted experiments. Even though the conversion varied and the reactor temperature sequence was not similar the achieved conversion is deemed to be within an acceptable range to confirm activity. At the reactor temperature of 1223 and 1273 K the methane conversion was significantly higher than obtained with an empty reactor for both the experiments featuring the Fe/HZSM-5 (1) catalyst, which is evidence of activity and indicates reproducibility.

## 5 FUTURE WORK

---

The synthesis of the Fe@SiO<sub>2</sub> catalyst was not optimal in this work according to the preparation method supplied by Guo et al. [4] However, it would be of interest to develop a different preparation method, that could bypass the need for fayalite completely, and thereby eliminating the potential source of error this synthesized material brings with it. If not, a better preparation of fayalite should be sought out, and the fayalite should be thoroughly characterized to assure that the source of error is kept as low as possible. An in-depth characterization of the catalyst could also be performed. EXAFS could be performed to examine the structure of the catalyst.

The Fe/HZSM-5 (1) catalyst that was synthesized after the instructions of Guo et al. [4] obtained a similar conversion as reported in the article. However, an equal product distribution could not be confirmed. Due to limitations in the analysis equipment, higher hydrocarbons such as benzene and naphthalene could not be detected. Improving the analysis of the product gas stream would give a greater insight into the product selectivity obtained by both the F2/HZSM-5 and Fe@SiO<sub>2</sub> catalyst. The spent catalyst along with the coke deposited on it can also be examined for traces of aromatics. The characteristics of the Fe/HZSM-5 catalyst could also be further investigated, to further confirm the Fe impregnation on the zeolite. The results of Tan [14] obtained from temperature-programmed desorption of ammonia (TPD-NH<sub>3</sub>), XRD and XPS could be used as a comparison to examine the success of the Fe impregnation.

Another possible avenue for improving the selectivity of the direct methane could be to design a more suitable reactor. Perhaps by limiting the dead space in the reactor the gas phase reactions that occur at high temperatures could be limited, which would result in a greater selectivity towards desired products. The challenge would lie in designing a small space for the catalyst while at the same time allowing for easy placement of the catalyst, as well as ensuring sufficient flow throughout the reactor and correct placement of the thermocouple.

## 6 CONCLUSION

---

The Fe@SiO<sub>2</sub> catalyst described in the article “*Nonoxidative conversion of methane to C<sub>2</sub> hydrocarbons, aromatics and hydrogen*” by Guo et al. [4] was prepared. Fayalite was one of the reagents used to prepare the catalyst, and it had to be synthesized. Characterization of the fayalite showed that the synthesis method was not adequate. The preparation method of the catalyst had significant deviations from what was described by Guo et al. [4], but the extent it would affect the catalyst activity and selectivity is unknown.

The prepared Fe/HZSM-5(1) catalyst displayed characteristics that correlated with Fe impregnation, which indicates that the preparation method was successful. The color of the catalyst after impregnation indicated that Fe loading was uneven, and that the catalyst was not homogenous. This was the same result for the Fe/HZSM-5 (2) catalyst, which was prepared by the more common incipient wetness method.

The HZSM-5 (1) and (2) catalysts showed activity at 1223 K temperature with a conversion of 16 and 19 %, opposed to 1 % conversion obtained with the empty reactor. The activity was also evident at 1273 K. When the reactor temperature was increased to 1323 K and 1373 K the conversion obtained during the blank experiment was similar to the catalyst driven experiments. This indicated that the gas phase reactions would have a great impact on the results at these temperatures. The calculated hydrogen loss demonstrated an inaccuracy in the analysis, therefore none of the results are definitive. Examination of the acetylene formation showed that as the reactor temperature increased, the selectivity towards acetylene increased as well. In fact, all measurements at all temperatures showed that there was production of acetylene. This was a major contradiction to what was reported by Guo et al. [4]

The conversion and product distribution obtained from the two zeolite catalysts and the blank experiment at 1223 K showed great similarity to what was reported by Guo et al. [4]

However, without the possibility of confirming the formation of aromatics, the results are not conclusive.

The Fe@SiO<sub>2</sub> catalyst was only examined at two temperatures, due to pressure buildup in the reactor. The methane conversion was not significantly different from the blank experiment results. This could be due to the deviances in the catalyst preparation, and therefore does not directly contradict the results obtained by Guo et al. [4] By comparing the product distribution at 1323 K obtained by the four experiments it could be seen that the Fe@SiO<sub>2</sub> catalyst achieved the most desired result. It had the greatest selectivity towards ethylene, and produced the least amount of coke. Further research into the formation of higher hydrocarbons should be conducted to confirm this. Though the conversion and selectivity were not in the same magnitude as what obtained by Guo et al. [4], the results obtained with the Fe@SiO<sub>2</sub> catalyst were promising. Further research such as improving the catalyst preparation and more thorough characterization of the catalyst should be performed to gain further insight into the Fe@SiO<sub>2</sub> catalyst.

## REFERENCES

---

1. Galadima, A. and O. Muraza, *Revisiting the oxidative coupling of methane to ethylene in the golden period of shale gas: A review*. Journal of Industrial and Engineering Chemistry.
2. Naturalgas.org. *Background*. [cited 2016 15.05]; Available from: <http://naturalgas.org/overview/background/>.
3. Holmen, A., *Direct conversion of methane to fuels and chemicals*. Catalysis Today, 2009. **142**(1): p. 2-8.
4. Guo, X., et al., *Direct, nonoxidative conversion of methane to ethylene, aromatics, and hydrogen*. Science, 2014. **344**(6184): p. 616-619.
5. Ruitenbeek, M. and B.M. Weckhuysen, *A Radical Twist to the Versatile Behavior of Iron in Selective Methane Activation*. Angewandte Chemie International Edition, 2014. **53**(42): p. 11137-11139.
6. Tang, P., et al., *Methane activation: the past and future*. Energy & Environmental Science, 2014. **7**(8): p. 2580-2591.
7. Karakaya, C. and R.J. Kee, *Progress in the direct catalytic conversion of methane to fuels and chemicals*. Progress in Energy and Combustion Science, 2016. **55**: p. 60-97.
8. Xu, Y., X. Bao, and L. Lin, *Direct conversion of methane under nonoxidative conditions*. Journal of Catalysis, 2003. **216**(1): p. 386-395.
9. Lunsford, J.H., *Catalytic conversion of methane to more useful chemicals and fuels: a challenge for the 21st century*. Catalysis Today, 2000. **63**(2): p. 165-174.
10. Chen, G.Q., T.J. Ahrens, and E. Stolper, *Shock-wave equation of state of molten and solid fayalite*. Physics of the Earth and Planetary Interiors, 2002. **134**(1): p. 35-52.
11. Daval, D., et al., *Fayalite (Fe<sub>2</sub>SiO<sub>4</sub>) dissolution kinetics determined by X-ray absorption spectroscopy*. Chemical geology, 2010. **275**(3): p. 161-175.
12. Akimoto, S.I. and H. Fujisawa, *Demonstration of the electrical conductivity jump produced by the olivine-spinel transition*. Journal of Geophysical Research, 1965. **70**(2): p. 443-449.
13. Daval, D., et al., *Fayalite (Fe<sub>2</sub>SiO<sub>4</sub>) dissolution kinetics determined by X-ray absorption spectroscopy*. Chemical Geology, 2010. **275**(3-4): p. 161-175.
14. Tan, P., *Active phase, catalytic activity, and induction period of Fe/zeolite material in nonoxidative aromatization of methane*. Journal of Catalysis, 2016. **338**: p. 21-29.
15. Chorkendorff, I. and J.W. Niemantsverdriet, *Concepts of modern catalysis and kinetics*. 2006: John Wiley & Sons.
16. science, E.m. *Molecular shape*. [cited 2016 06.06]; Available from: <http://www.everythingmaths.co.za/science/grade-11/03-atomic-combinations/03-atomic-combinations-02.cnxmplus>.
17. Hunt, D.H.K. *Biophotonics*. 2010; Available from: <http://web.missouri.edu/~hunthk/Research.html>.
18. Busca, G., *Chapter 7 - Zeolites and Other Structurally Microporous Solids as Acid-Base Materials*, in *Heterogeneous Catalytic Materials*. 2014, Elsevier: Amsterdam. p. 197-249.

19. University, O. *The atomic basis of matter*. 1996 [cited 2016 01.06]; Available from: [http://www.met.reading.ac.uk/pplato2/h-flap/phys7\\_1.html](http://www.met.reading.ac.uk/pplato2/h-flap/phys7_1.html).
20. Analytical, P. *Brunauer, Emmett and Teller (BET) Theory*. 2016 [cited 2016 19.05]; Available from: <http://particle.dk/methods-analytical-laboratory/surface-area-bet/surface-area-bet-theory/>.
21. Micromeritics. *Gas sorption analysis*. 2001 [cited 2016 19.05]; Available from: [http://www.micromeritics.com/Repository/Files/Gas\\_Sorption.pdf](http://www.micromeritics.com/Repository/Files/Gas_Sorption.pdf).
22. Services, W.S. *Surface area and porosity analysis*. 2014 [cited 2016 06.06]; Available from: <http://www2.warwick.ac.uk/services/ris/impactinnovation/impact/analyticalguide/porosimetry/>.
23. Technologies, A. *HP-PLOT Q*. 2016; Available from: <https://www.agilent.com/en-us/products/gas-chromatography/gc-columns/capillary/hp-plot-q>.

# APPENDIX A - FLOW CONTROLLER CALIBRATION

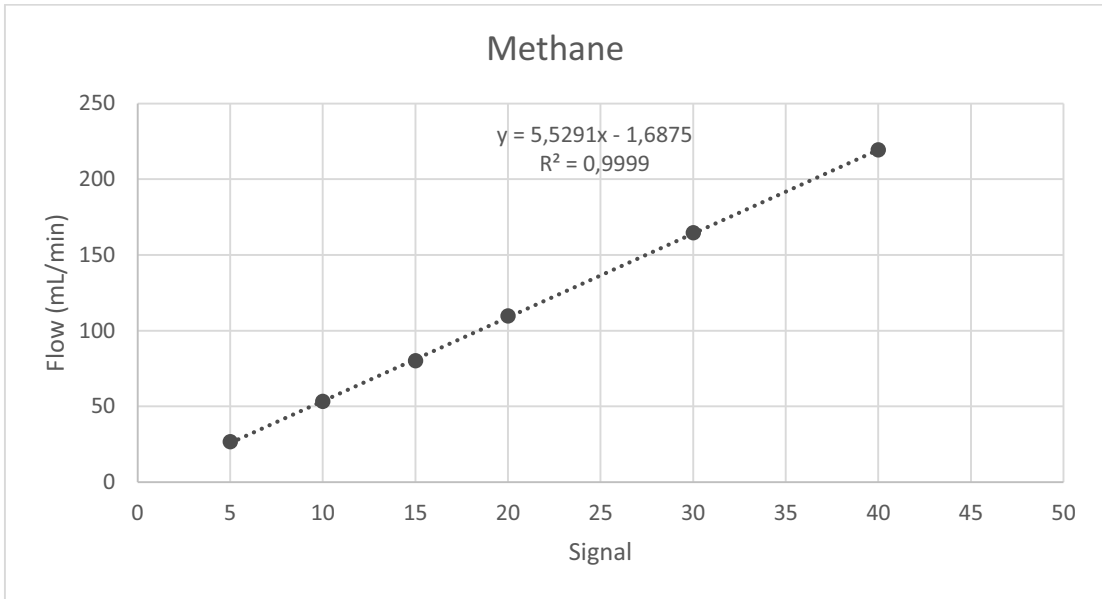


Figure A 1: Calibration curve for the methane flow controller

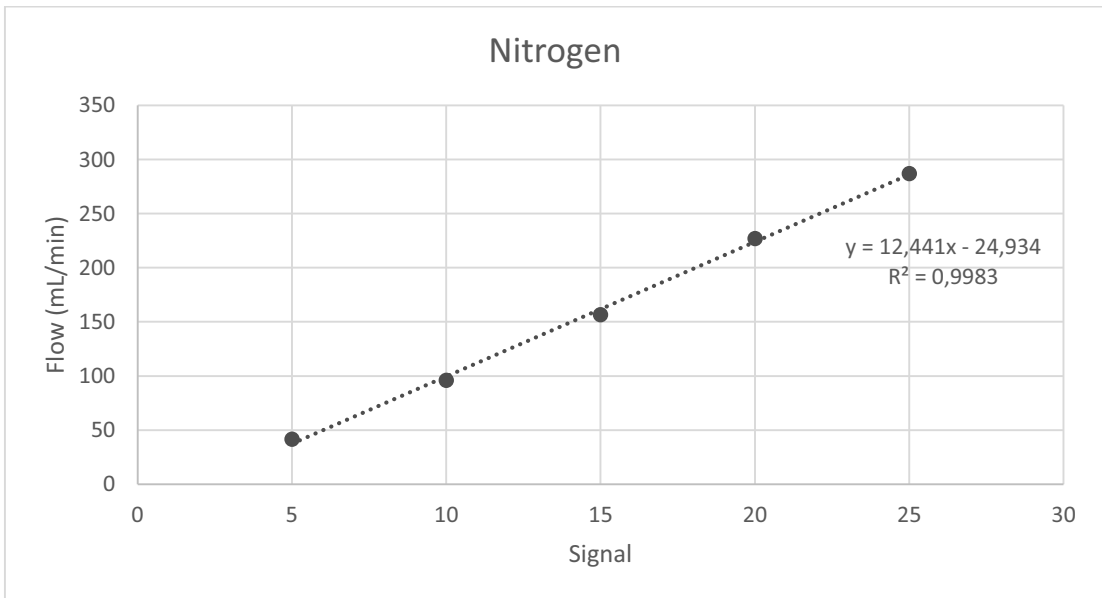


Figure A 2: Calibration curve for the nitrogen flow controller

## APPENDIX B – $\mu$ GC CALIBRATION

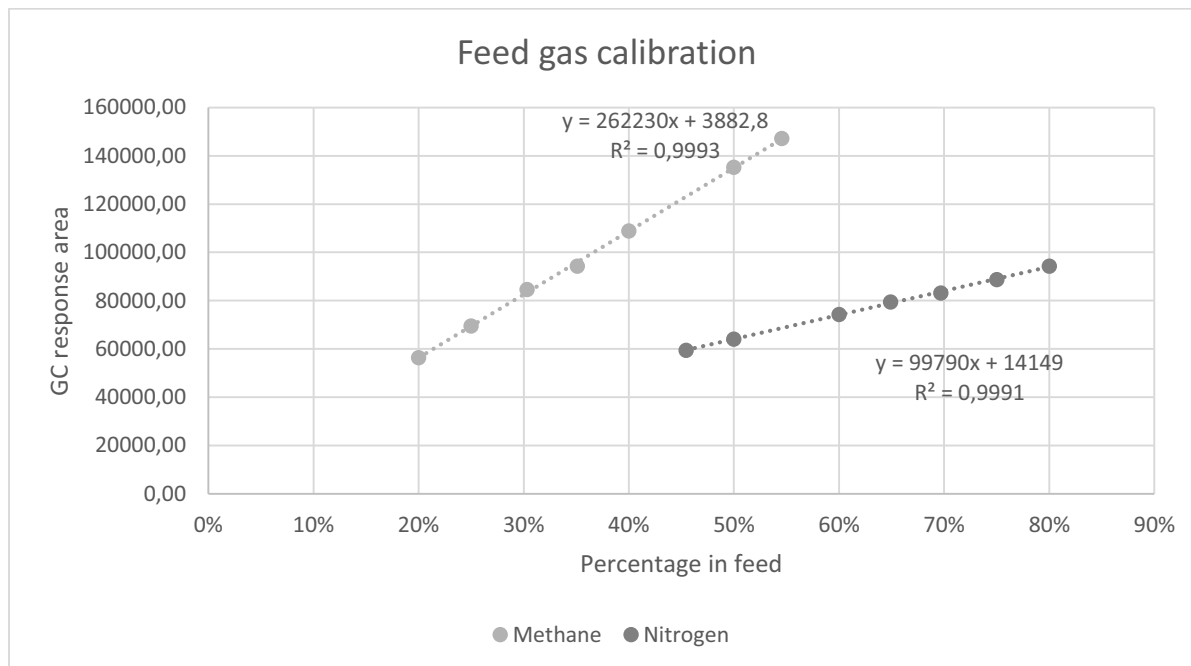


Figure B 1: Calibration curves for methane and nitrogen.

Table B 1:  $\mu$ GC equations obtained by calibration of the  $\mu$ GC.

<b><math>\mu</math>GC equations</b>	
<b>Compound</b>	<b>Equation</b>
Nitrogen	$x = (y-14149)/99790$
Methane	$x = (y-3882,8)/262230$
Hydrogen	$x = (y+14578,97)/1427216$
Ethane	$x = (y+12,27)/ 3567704$
Ethylene	$x = y +12,27/ 5913291$
Acetylene	$x = y/3170284$

## APPENDIX C - SEPARATION OF ACETYLENE AND ETHYLENE

---

The initial  $\mu$ GC set points that were used are shown in the table below.

*Table C 1: Set points for the  $\mu$ GC that was used during the initial experiments.*

<b><math>\mu</math>GC set point</b>	<b>Molecular sieve</b>	<b>PLOT Q</b>
Inlet temperature[C]	120	120
Injector temperature [C]	95	85
Column temperature [C]	95	85
Run time	125	125
Column pressure [psi]	36.00	48.00

The molecular sieve column could separate nitrogen, methane and hydrogen. Ethane, ethylene and acetylene should in theory be separated by the PLOT Q column. By using a feed consisting of a calibration gas with a known composition it was established that ethane and ethylene was successfully separated.

By using the GasMix a feed consisting of nitrogen, ethylene and acetylene was fed to the  $\mu$ GC. For a successful separation there should be 3 peaks detected from the PLOT Q column, in the elution order of nitrogen, ethylene and acetylene. However, it became apparent that apart from the nitrogen peak, only one other peak was observed. This confirmed that ethylene and acetylene was not separated, and would eluate together by using the aforementioned conditions.

To obtain a separation of ethylene and acetylene some of the  $\mu$ GC set points were altered. The pressure was lowered to 25.00 psi, and the temperature was lowered as well. A few different temperatures were tested to see when the separation could be achieved. In the figure below three different chromatograms are shown for respectively 60, 50 and 40 °C.

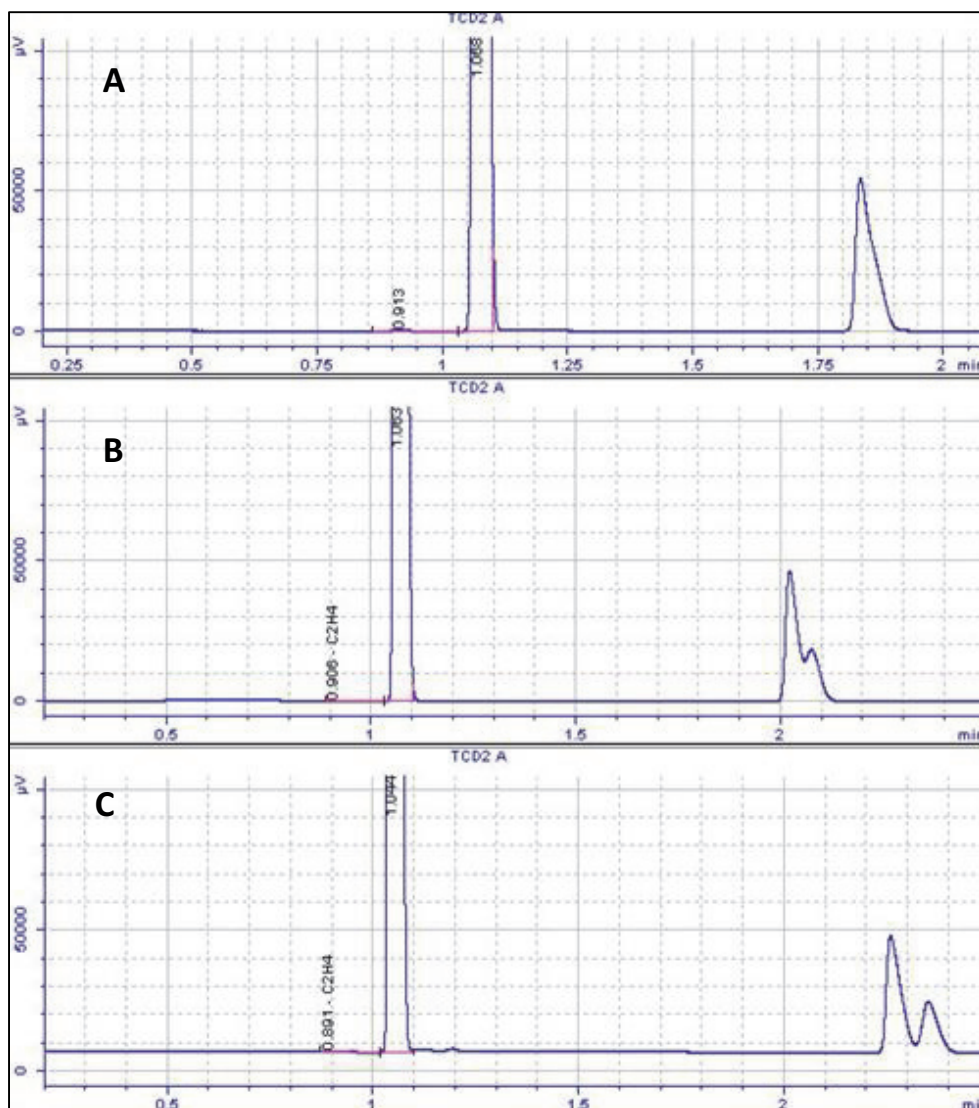


Figure C 1: Chromatograms obtained at 60 (A), 50 (B) and 42 (C) °C.

The three chromatograms show that at 60 °C there is no separation, but when the column temperature is lowered to 50 °C there is a partial separation and a double peak appears. As the temperature further decreases the separation of ethylene and acetylene is more successful. It was attempted to lower the column temperature to 40 °C, but the lowest obtainable temperature was 42 °C. As shown in the chromatogram marked C the separation here was near complete, and the two compounds could be identified and quantified. However, since the separation wasn't complete, the quantification of ethylene and acetylene

has an element of uncertainty to it. Below is an illustration of how the areas of the two peaks were divided.

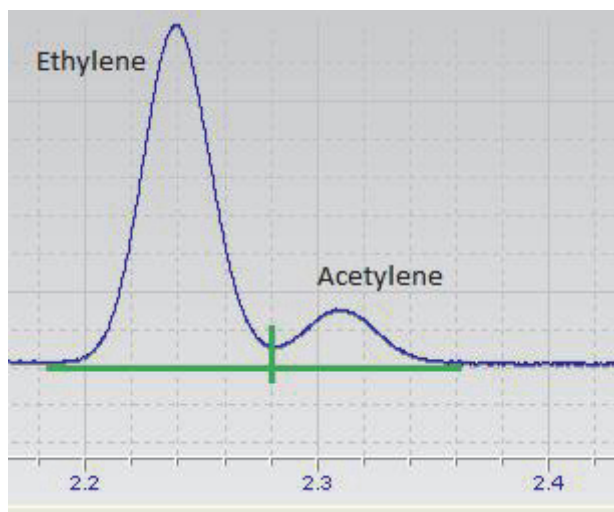


Figure C 2: An illustration of how the  $\mu$ GC area for ethylene and acetylene was separated for the area calculation.

The new  $\mu$ GC set points that were used for all measurements is shown in the table below. Only the values for the PLOT Q column was changed. Note that the run time was prolonged due to the lowering of pressure and temperature.

Table C 2: The  $\mu$ GC set points that were used for all experiments.

<b><math>\mu</math>GC set point</b>	<b>Molecular sieve</b>	<b>PLOT Q</b>
Inlet temperature[C]	120	120
Injector temperature [C]	95	42
Column temperature [C]	95	42
Run time	125	180
Column pressure [psi]	36.00	25.00

# APPENDIX D – RISK EVALUATION

---



## Detaljert Risikoreport

<b>ID</b>	1717	<b>Status</b>	<b>Dato</b>
<b>Risikoområde</b>	Risikovurdering: Helse, miljø og sikkerhet (HMS)	Opprettet	09.11.2015
<b>Opprettet av</b>	Cristian Ledesma Rodriguez	Vurdering startet	09.11.2015
<b>Ansvarlig</b>	Benedicte Hovd	Tiltak besluttet	
		Avsluttet	

**CAT, Master student 2016, Benedicte Hovd**

### Gyldig i perioden:

10/7/2015 - 7/1/2016

### Sted:

3 - Gløshaugen / 315 - Kjemi 5

### Mål / hensikt

This risk assessment contains all the activities that the master student Benedicte Hovd will perform in the labs of the Catalysis group. The preparation of the catalysts is carried out in K5-228 and the catalysts are afterwards tested in Chemistry Hall D 2nd floor (unit 2.4). The project consist of direct conversion of methane to C2 hydrocarbons.

### Bakgrunn

[Ingen registreringer]

### Beskrivelse og avgrensninger

### Forutsetninger, antakelser og forenklinger

[Ingen registreringer]

### Vedlegg

[Ingen registreringer]

### Referanser

[Ingen registreringer]

Norges teknisk-naturvitenskapelige universitet (NTNU)

Unntatt offentlighet jf. Offentlighetsloven § 14

Utskriftsdato:

22.05.2016

Utskrift foretatt av:

Benedicte Hovd

Side:

1/16

**Oppsummering, resultat og endelig vurdering**

I oppsummeringen presenteres en oversikt over farer og uønskede hendelser, samt resultat for det enkelte konsekvensområdet.

**Farekilde:** Use of ball mill**Uønsket hendelse:** Inhalation of small particles

<b>Konsekvensområde:</b> Helse	Risiko før tiltak:		Risiko etter tiltak:	
Ytre miljø	Risiko før tiltak:		Risiko etter tiltak:	
Materielle verdier	Risiko før tiltak:		Risiko etter tiltak:	

**Farekilde:** Use of high temperature furnace**Uønsket hendelse:** Electric shock

<b>Konsekvensområde:</b> Helse	Risiko før tiltak:		Risiko etter tiltak:	
Ytre miljø	Risiko før tiltak:		Risiko etter tiltak:	
Materielle verdier	Risiko før tiltak:		Risiko etter tiltak:	

**Uønsket hendelse:** Uncontrolled heating

<b>Konsekvensområde:</b> Helse	Risiko før tiltak:		Risiko etter tiltak:	
Ytre miljø	Risiko før tiltak:		Risiko etter tiltak:	
Materielle verdier	Risiko før tiltak:		Risiko etter tiltak:	

**Uønsket hendelse:** Fire

<b>Konsekvensområde:</b> Helse	Risiko før tiltak:		Risiko etter tiltak:	
Ytre miljø	Risiko før tiltak:		Risiko etter tiltak:	
Materielle verdier	Risiko før tiltak:		Risiko etter tiltak:	



**Uønsket hendelse:** Burn damage

<b>Konsekvensområde:</b> Helse	Risiko før tiltak: ●	Risiko etter tiltak: ●
Ytre miljø	Risiko før tiltak: ●	Risiko etter tiltak: ●
Materielle verdier	Risiko før tiltak: ●	Risiko etter tiltak: ●

**Farekilde:** Use of corrosive chemicals (HNO3)

---

**Uønsket hendelse:** Spills on skin

<b>Konsekvensområde:</b> Helse	Risiko før tiltak: ●	Risiko etter tiltak: ●
Ytre miljø	Risiko før tiltak: ●	Risiko etter tiltak: ●
Materielle verdier	Risiko før tiltak: ●	Risiko etter tiltak: ●

**Farekilde:** Use of compressed gases (N2, Ar)

---

**Uønsket hendelse:** Uncontrolled expansion and depletion of O2

<b>Konsekvensområde:</b> Helse	Risiko før tiltak: ●	Risiko etter tiltak: ●
Ytre miljø	Risiko før tiltak: ●	Risiko etter tiltak: ●
Materielle verdier	Risiko før tiltak: ●	Risiko etter tiltak: ●

**Uønsket hendelse:** Gas leakage

<b>Konsekvensområde:</b> Helse	Risiko før tiltak: ●	Risiko etter tiltak: ●
Ytre miljø	Risiko før tiltak: ●	Risiko etter tiltak: ●
Materielle verdier	Risiko før tiltak: ●	Risiko etter tiltak: ●



**Farekilde:** Use of flammable gases (CH4)

---

**Uønsket hendelse:** Gas leakage

**Konsekvensområde:** Helse

Risiko før tiltak:  Risiko etter tiltak: 

Ytre miljø

Risiko før tiltak:  Risiko etter tiltak: 

Materielle verdier

Risiko før tiltak:  Risiko etter tiltak: 

**Uønsket hendelse:** Fire, explosion

**Konsekvensområde:** Helse

Risiko før tiltak:  Risiko etter tiltak: 

Ytre miljø

Risiko før tiltak:  Risiko etter tiltak: 

Materielle verdier

Risiko før tiltak:  Risiko etter tiltak: 



Endelig vurdering



### Oversikt involverte enheter og personell

En risikovurdering kan gjelde for en, eller flere enheter i organisasjonen. Denne oversikten presenterer involverte enheter og personell for gjeldende risikovurdering.

#### Enhet /-er risikovurderingen omfatter

- Institutt for kjemisk prosesssteknologi

#### Deltakere

Cristian Ledesma Rodriguez

Karin Wiggen Dragsten

Hilde Johnsen Venvik

#### Lesere

[Ingen registreringer]

#### Andre involverte/interessenter

[Ingen registreringer]

Følgende akseptkriterier er besluttet for risikoområdet Risikovurdering: Helse, miljø og sikkerhet (HMS):

#### Helse



#### Materielle verdier



#### Omdømme



#### Ytre miljø



**Oversikt over eksisterende, relevante tiltak som er hensyntatt i risikovurderingen**

I tabellen under presenteres eksisterende tiltak som er hensyntatt ved vurdering av sannsynlighet og konsekvens for aktuelle uønskede hendelser.

<b>Farekilde</b>	<b>Uønsket hendelse</b>	<b>Tiltak hensyntatt ved vurdering</b>	
Use of ball mill	Inhalation of small particles	HSE documentation	
	Inhalation of small particles	Working alone regulations at NTNU	
	Inhalation of small particles	Personal protective equipment	
Use of high temperature furnace	Electric shock	HSE documentation	
	Electric shock	Working alone regulations at NTNU	
	Electric shock	Personal protective equipment	
	Uncontrolled heating	HSE documentation	
	Uncontrolled heating	Working alone regulations at NTNU	
	Uncontrolled heating	Personal protective equipment	
	Fire	HSE documentation	
	Fire	Working alone regulations at NTNU	
	Fire	Personal protective equipment	
	Fire	Ventilation	
Use of corrosive chemicals (HNO <sub>3</sub> )	Spills on skin	HSE documentation	
	Spills on skin	Working alone regulations at NTNU	
	Spills on skin	Personal protective equipment	
	Spills on skin	Ventilation	
	Use of compressed gases (N <sub>2</sub> , Ar)	Uncontrolled expansion and depletion of O <sub>2</sub>	HSE documentation
		Uncontrolled expansion and depletion of O <sub>2</sub>	Working alone regulations at NTNU
		Uncontrolled expansion and depletion of O <sub>2</sub>	Personal protective equipment
		Uncontrolled expansion and depletion of O <sub>2</sub>	Ventilation
Uncontrolled expansion and depletion of O <sub>2</sub>		Leak test procedure	
Uncontrolled expansion and depletion of O <sub>2</sub>		Installation and change of gas cylinders	
Gas leakage		HSE documentation	



	Gas leakage	Working alone regulations at NTNU
	Gas leakage	Personal protective equipment
	Gas leakage	Ventilation
	Gas leakage	Leak test procedure
	Gas leakage	Installation and change of gas cylinders
Use of flammable gases (CH <sub>4</sub> )	Gas leakage	HSE documentation
	Gas leakage	Working alone regulations at NTNU
	Gas leakage	Personal protective equipment
	Gas leakage	Ventilation
	Gas leakage	Gas detectors
	Gas leakage	Leak test procedure
	Gas leakage	Installation and change of gas cylinders
	Fire, explosion	HSE documentation
	Fire, explosion	Working alone regulations at NTNU
	Fire, explosion	Personal protective equipment
	Fire, explosion	Ventilation
	Fire, explosion	Gas detectors
	Fire, explosion	Leak test procedure
	Fire, explosion	Installation and change of gas cylinders

**Eksisterende og relevante tiltak med beskrivelse:****HSE documentation**

The laboratories have an updated Room Card and the unit 2.4 has a copy of the risk assessment, operating instructions and apparatus card with information regarding safety and information in case of emergency stop.

Different phone numbers are provided to contact in case of emergency.

**Working alone regulations at NTNU**

NTNU students and employee are not allowed to work alone after 7pm and during the weekends.

Working after 19:00 or in the weekends, you need to be at least 2 in the lab or in the building with regularly check-ups (every 30 minutes). Both of the people needs to have access to the labs

**Personal protective equipment**

The hall contains googles, other safety measures and a first-aid kit.. There are also gloves, lab coats and more protective equipment available upon request.

**Ventilation**

The reactor system is installed inside a cabinet with ventilation.

**Gas detectors**

The cabinet has CO/H<sub>2</sub> and CH<sub>4</sub>/H<sub>2</sub> detectors which trigger the alarms in case of leakage. There are portable detectors that must be used during the leak tests before running experiments.



**Leak test procedure**

Before running experiments, a leak test must be performed following the procedure attached.

**Installation and change of gas cylinders**

This will be done by authorized personnel only.

**Risikoanalyse med vurdering av sannsynlighet og konsekvens**

I denne delen av rapporten presenteres detaljer dokumentasjon av de farer, uønskede hendelser og årsaker som er vurdert. Innledningsvis oppsummeres farer med tilhørende uønskede hendelser som er tatt med i vurderingen.

**Følgende farer og uønskede hendelser er vurdert i denne risikovurderingen:**

- **Use of ball mill**
  - Inhalation of small particles
  
- **Use of high temperature furnace**
  - Electric shock
  - Uncontrolled heating
  - Fire
  - Burn damage
  
- **Use of corrosive chemicals (HNO<sub>3</sub>)**
  - Spills on skin
  
- **Use of compressed gases (N<sub>2</sub>, Ar)**
  - Uncontrolled expansion and depletion of O<sub>2</sub>
  - Gas leakage
  
- **Use of flammable gases (CH<sub>4</sub>)**
  - Gas leakage
  - Fire, explosion

**Oversikt over besluttede risikoreducerende tiltak med beskrivelse:**

**Use of ball mill (farekilde)**

Norges teknisk-naturvitenskapelige universitet (NTNU)

Unntatt offentlighet jf. Offentlighetsloven § 14

Utskriftsdato:

22.05.2016

Utskrift foretatt av:

Benedicte Hovd

Side:

9/16



**Use of ball mill/Inhalation of small particles (uønsket hendelse)**

Samlet sannsynlighet vurdert for hendelsen: Sannsynlig (3)

Kommentar til vurdering av sannsynlighet:

It is necessary to use dust mask

**Vurdering av risiko for følgende konsekvensområde: Helse**

Vurdert sannsynlighet (felles for hendelsen): Sannsynlig (3)

Vurdert konsekvens: Middels (2)

Kommentar til vurdering av konsekvens:

[Ingen registreringer]



**Use of high temperature furnace (farekilde)**

**Use of high temperature furnace/Electric shock (uønsket hendelse)**

Samlet sannsynlighet vurdert for hendelsen: Svært lite sannsynlig (1)

Kommentar til vurdering av sannsynlighet:

[Ingen registreringer]

**Vurdering av risiko for følgende konsekvensområde: Helse**

Vurdert sannsynlighet (felles for hendelsen): Svært lite sannsynlig (1)

Vurdert konsekvens: Middels (2)

Kommentar til vurdering av konsekvens:

[Ingen registreringer]





**Use of high temperature furnace/Uncontrolled heating (uønsket hendelse)**

Samlet sannsynlighet vurdert for hendelsen: Svært lite sannsynlig (1)

Kommentar til vurdering av sannsynlighet:

[Ingen registreringer]

**Vurdering av risiko for følgende konsekvensområde: Helse**

Vurdert sannsynlighet (felles for hendelsen): Svært lite sannsynlig (1)

Vurdert konsekvens: Middels (2)

Kommentar til vurdering av konsekvens:

[Ingen registreringer]



**Use of high temperature furnace/Fire (uønsket hendelse)**

Samlet sannsynlighet vurdert for hendelsen: Svært lite sannsynlig (1)

Kommentar til vurdering av sannsynlighet:

[Ingen registreringer]

**Vurdering av risiko for følgende konsekvensområde: Helse**

Vurdert sannsynlighet (felles for hendelsen): Svært lite sannsynlig (1)

Vurdert konsekvens: Stor (3)

Kommentar til vurdering av konsekvens:

[Ingen registreringer]





**Use of high temperature furnace/Burn damage (uønsket hendelse)**

Samlet sannsynlighet vurdert for hendelsen: Lite sannsynlig (2)

Kommentar til vurdering av sannsynlighet:

[Ingen registreringer]

**Vurdering av risiko for følgende konsekvensområde: Helse**

Vurdert sannsynlighet (felles for hendelsen): Lite sannsynlig (2)

Vurdert konsekvens: Middels (2)

Kommentar til vurdering av konsekvens:

[Ingen registreringer]



**Use of corrosive chemicals (HNO3) (farekilde)**

**Use of corrosive chemicals (HNO3)/Spills on skin (uønsket hendelse)**

Samlet sannsynlighet vurdert for hendelsen: Lite sannsynlig (2)

Kommentar til vurdering av sannsynlighet:

[Ingen registreringer]

**Vurdering av risiko for følgende konsekvensområde: Helse**

Vurdert sannsynlighet (felles for hendelsen): Lite sannsynlig (2)

Vurdert konsekvens: Middels (2)

Kommentar til vurdering av konsekvens:

[Ingen registreringer]



**Use of compressed gases (N2, Ar) (farekilde)**



**Use of compressed gases (N<sub>2</sub>, Ar)/Uncontrolled expansion and depletion of O<sub>2</sub> (uønsket hendelse)**

Samlet sannsynlighet vurdert for hendelsen: Lite sannsynlig (2)

Kommentar til vurdering av sannsynlighet:

[Ingen registreringer]

**Vurdering av risiko for følgende konsekvensområde: Helse**

Vurdert sannsynlighet (felles for hendelsen): Lite sannsynlig (2)

Vurdert konsekvens: Stor (3)

Kommentar til vurdering av konsekvens:

[Ingen registreringer]



**Use of compressed gases (N<sub>2</sub>, Ar)/Gas leakage (uønsket hendelse)**

Samlet sannsynlighet vurdert for hendelsen: Svært lite sannsynlig (1)

Kommentar til vurdering av sannsynlighet:

[Ingen registreringer]

**Vurdering av risiko for følgende konsekvensområde: Helse**

Vurdert sannsynlighet (felles for hendelsen): Svært lite sannsynlig (1)

Vurdert konsekvens: Middels (2)

Kommentar til vurdering av konsekvens:

[Ingen registreringer]



**Use of flammable gases (CH<sub>4</sub>) (farekilde)**



**Use of flammable gases (CH<sub>4</sub>)/Gas leakage (uønsket hendelse)**

Samlet sannsynlighet vurdert for hendelsen: Lite sannsynlig (2)

Kommentar til vurdering av sannsynlighet:

[Ingen registreringer]

**Vurdering av risiko for følgende konsekvensområde: Helse**

Vurdert sannsynlighet (felles for hendelsen): Lite sannsynlig (2)

Vurdert konsekvens: Stor (3)

Kommentar til vurdering av konsekvens:

[Ingen registreringer]



**Use of flammable gases (CH<sub>4</sub>)/Fire, explosion (uønsket hendelse)**

Samlet sannsynlighet vurdert for hendelsen: Lite sannsynlig (2)

Kommentar til vurdering av sannsynlighet:

[Ingen registreringer]

**Vurdering av risiko for følgende konsekvensområde: Helse**

Vurdert sannsynlighet (felles for hendelsen): Lite sannsynlig (2)

Vurdert konsekvens: Stor (3)

Kommentar til vurdering av konsekvens:

[Ingen registreringer]





**Oversikt over besluttede risikoreducerende tiltak:**

Under presenteres en oversikt over risikoreducerende tiltak som skal bidra til å reduseres sannsynlighet og/eller konsekvens for uønskede hendelser.

**Oversikt over besluttede risikoreducerende tiltak med beskrivelse:**

